bound form of many Rab proteins (*20*, *21*). We thus examined whether protrudin actually interacted with Rab11. Endogenous protrudin did indeed interact with endogenous Rab11 in PC12 cells, and this interaction was enhanced by NGF treatment (Fig. 3B). FLAG-protrudin also interacted with hemagglutinin (HA)–tagged Rab11 in human embryonic kidney (HEK293T) cells (Fig. 3C). Protrudin preferentially interacted with the GDP-bound form of Rab11 [as represented by the GTP binding–deficient mutant $Ser^{25}\rightarrow Asn^{25}$ (S25N)] rather than with the GTP-bound form [as represented by the GTPase-deficient mutant $Gln^{70}\rightarrow Leu^{70}$ (Q70L)] (*22*, *23*) (Fig. 3D). The RBD11 of the Rab11 effector FIP2 interacted specifically with Rab11-GTP, whereas the RBD11 of protrudin specifically interacted with Rab11-GDP (fig. S4A). Reciprocal co-immunoprecipitation analysis as well as an in vitro pull-down assay confirmed that protrudin preferentially interacts with Rab11-GDP (fig. S4, B and C). We also generated a series of deletion mutants of protrudin (fig. S1B) and tested them for the ability to bind Rab11. Rab11(S25N) interacted with the N1 mutant but not with the ΔRBD-N1 mutant (fig. S4D). Furthermore, a protrudin deletion mutant lacking the RBD11 (ΔRBD in fig. S1B) could not restore neurite formation in PC12 cells depleted of protrudin by RNAi (fig. S5A) or induce process formation in HeLa cells (fig. S5B). Thus, protrudin preferentially binds to Rab11-GDP, and this association is required for neurite formation.

Sustained activation of the mitogen-activated protein kinase (MAPK) ERK accompanies NGF-dependent neurite extension in PC12 cells (*24*) (fig. S6A). PC12 cells expressing a constitutively active form of MEK1 [MEK1(SDSE)], which activated ERK, manifested neurite formation in the absence of NGF (fig. S6, B and C). Protrudin and MEK1(SDSE) showed a synergistic effect on process formation in HeLa cells, whereas a kinase-negative form of MEK1 [MEK1(K97S)] antagonized the process-forming activity of protrudin (fig. S6D). Protrudin contains six potential ERK phosphorylation sites as well as two consensus ERK binding (ERK D) domains (fig. S1C). Phosphorylation of protrudin was increased by NGF treatment or MEK1(SDSE) expression, but not by MEK1(K97S) expression, in PC12 cells (Fig. 3E). Two-dimensional polyacrylamide gel electrophoresis (2D-PAGE) also suggested that protrudin is phosphorylated by ERK in response to NGF (Fig. 3F). MEK1(K97S) expression inhibited the NGF-induced shift, suggesting that ERK activation is essential for the phosphorylation of protrudin elicited by NGF.

We examined the effect of ERK activation on protrudin-Rab11 interaction in HEK293T cells. Expression of MEK1(SDSE) enhanced the interaction between protrudin and Rab11(S25N) (Fig. 3G). At high amounts of MEK1(SDSE) expression, both wild-type and S25N forms of Rab11 interacted substantially with protrudin (fig. S7, A and B). Furthermore, protrudin mutants that lack some of potential ERK phosphorylation sites (P-mut-1 and -4) or both intact ERK D domains (D-mut) (fig. S1C) showed markedly reduced affinities for Rab11 compared with the affinities of wild-type protrudin (Fig. 3H and fig. S7C). Replacement of potential ERK phosphorylation sites in other combinations (P-mut-2 and -3) did not affect the binding (fig. S7D). Thus, phosphorylation of protrudin at multiple sites in response to NGF-ERK signaling promotes its interaction with Rab11.

We next investigated the effect of Rab11 on the morphology of PC12 cells. The morphology of cells expressing Rab11(Q70L) appeared nearly identical to that of cells depleted of endogenous protrudin (Fig. 4A). Conversely, the phenotype conferred by expression of Rab11(S25N) was similar to that conferred by expression of protrudin. These experiments were combined to examine the genetic relation between protrudin and Rab11. Expression of Rab11(S25N) induced neurite formation in cells depleted of endogenous protrudin (Fig. 4B), whereas overexpression of protrudin had no effect on the morphology of cells expressing Rab11(Q70L) (Fig. 4C). In addition, expression of Rab11(Q70L) inhibited process formation induced by protrudin in HeLa cells (movie S2). Thus, protrudin is indeed an upstream inhibitor of Rab11 function.

To investigate the role of the protrudin-Rab11 system in directed membrane traffic, we observed the transport of NgCAM, a cell adhesion molecule that is delivered to the somatodendritic plasma membrane and then transported to the axonal plasma membrane via recycling endosomes (*25*–*27*). Chicken NgCAM expressed in PC12 cells initially accumulated, presumably in the endoplasmic reticulum–Golgi compartment, and was subsequently transported to the plasma membrane of some neurites, but not to that of the soma, in the presence of NGF (Fig. 4D and fig. S8). In contrast, cells depleted of protrudin by RNAi or those expressing Rab11(Q70L) exhibited prominent surface

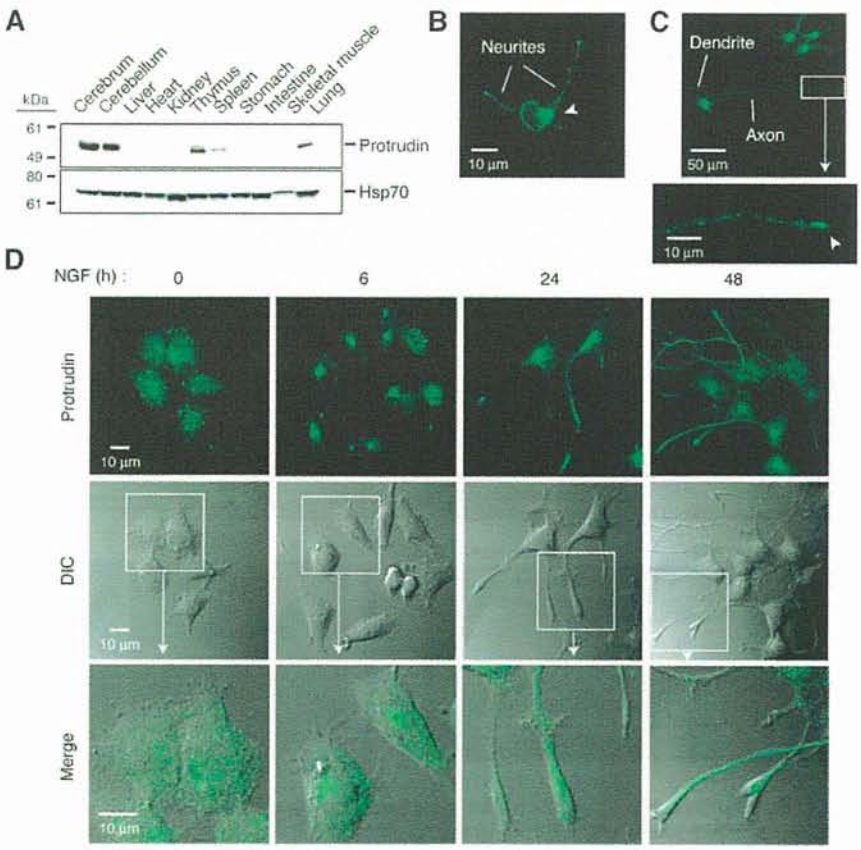


**Fig. 2.** Subcellular redistribution of protrudin during neuritogenesis. **(A)** Tissue distribution of protrudin in mice. **(B and C)** Cells isolated from embryonic mouse cerebral cortex were cultured for 1 (B) or 3 (C) days and stained with anti-protrudin (green). Arrowhead in (B) indicates the pericentrosomal region. The boxed region in (C) is shown at higher magnification in the bottom image; the arrowhead indicates the growth cone. **(D)** PC12 cells were incubated with NGF and stained with anti-protrudin (top, green). Differential interference contrast (DIC) images are shown in the middle, and the boxed regions are shown at bottom merged with protrudin.

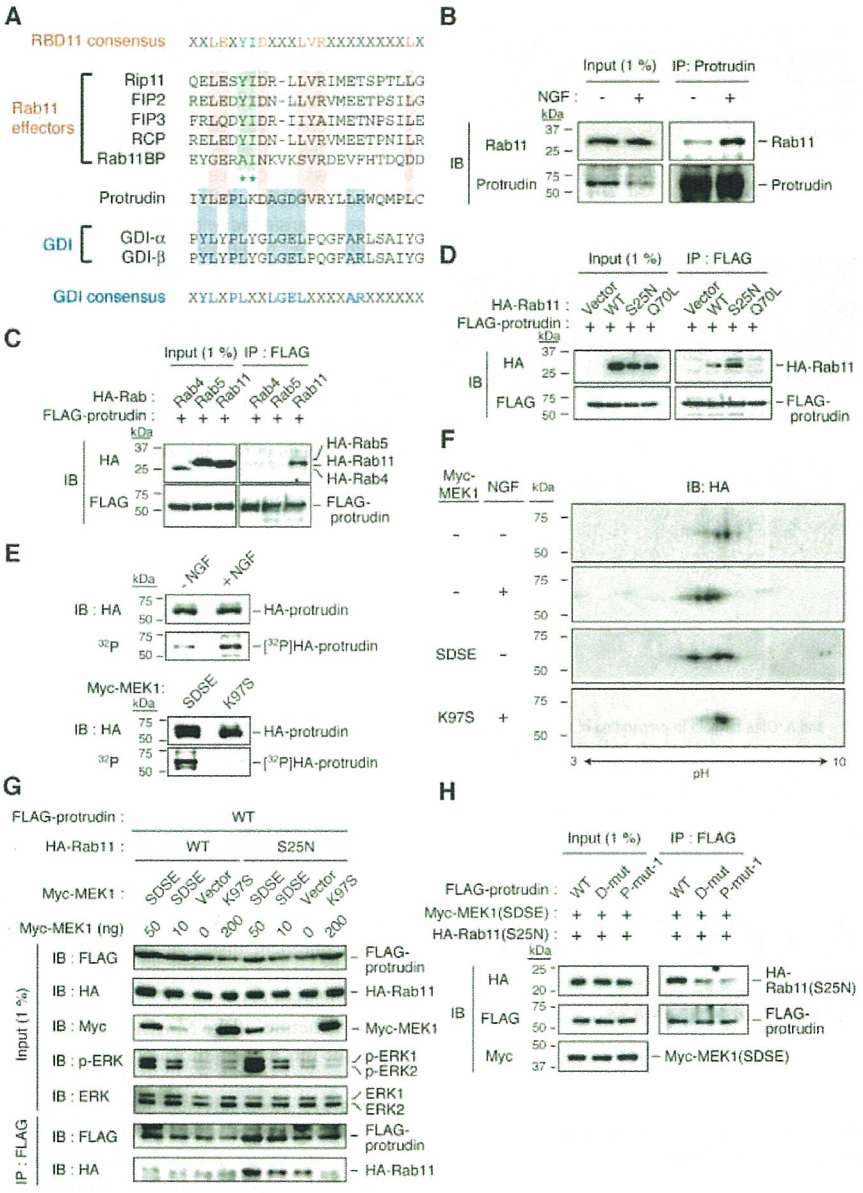


**Fig. 3.** Interaction of protrudin with Rab11. **(A)** Alignment of the amino acid sequence (*17*) of the RBD11 of protrudin with the Rab11 effector proteins and GDIs. Conserved residues are shaded in red or blue. Asterisks denote critical residues for interaction with Rab11-GTP (shaded in green). **(B)** Immunoprecipitation (IP) of PC12 lysates with anti-protrudin and immunoblotting (IB) with anti-Rab11 and -protrudin. **(C)** FLAG-protrudin expressed with HA-Rab4, -Rab5, or -Rab11 in HEK293T cells was immunoprecipitated and subjected to IB with anti-HA and -FLAG. **(D)** FLAG-protrudin expressed with either wild-type (WT) or mutant (S25N or Q70L) HA-Rab11 in HEK293T cells was immunoprecipitated and subjected to IB with anti-HA and -FLAG. **(E)** PC12 cells expressing HA-protrudin were metabolically labeled with [$^{32}$P]orthophosphate in the absence or presence of NGF (top). Alternatively, PC12 cells expressing HA-protrudin and Myc-MEK1 (SDSE or K97S) were similarly labeled (bottom). Cell lysates were subjected to IP with anti-HA and to autoradiography or to IB with anti-HA. **(F)** PC12 cells expressing HA-protrudin as well as Myc-MEK1 (SDSE or K97S) were incubated with or without NGF. Cell lysates were subjected to IP with anti-HA and to 2D-PAGE followed by IB with anti-HA. **(G)** HEK293T cells transfected with FLAG-protrudin, HA-Rab11 (WT or S25N), and Myc-MEK1 (SDSE or K97S) were subjected to IP with anti-FLAG and to IB with anti-FLAG, -HA, -Myc, -ERK, and -phospho-ERK (p-ERK). **(H)** HEK293T cells transfected with FLAG-protrudin (WT, D-mut, or P-mut-1), Myc-MEK1(SDSE), and HA-Rab11(S25N) were subjected to IP with anti-FLAG and to IB with anti-HA, -FLAG, and -Myc.

expression of NgCAM on the soma (Fig. 4D). Thus, protrudin is essential for directional membrane trafficking to neurites.

Our data indicate that the protrudin-Rab11 system is an important determinant of the direction of membrane trafficking and neurite formation. It was recently shown that ZFYVE27 (a synonym of protrudin) is mutated in a German family with an autosomal dominant form of hereditary spastic paraplegia (AD-HSP), which is characterized by selective degeneration of axons (*28*). The phenotype of the affected individuals was similar to that of patients with AD-HSP caused by mutation of spastin, a protein implicated in neuronal vesicular cargo trafficking. Protrudin is thought to interact with spastin via its FYVE domain in the COOH-terminal region of the protein. This genetic evidence supports our conclusion that protrudin plays a central role in membrane trafficking in neurons. Rab11, protrudin, and spastin may together constitute a system for the regulation of vesicular transport in neurons, and impairment of this system may be responsible for the pathogenesis of AD-HSP.

### References and Notes


1. L. S. Goldstein, Z. Yang, *Annu. Rev. Neurosci.* **23**, 39 (2000).
2. A. M. Craig, G. Banker, *Annu. Rev. Neurosci.* **17**, 267 (1994).
3. A. H. Futerman, G. A. Banker, *Trends Neurosci.* **19**, 144 (1996).
4. B. L. Tang, *J. Neurochem.* **79**, 923 (2001).
5. R. Behnia, S. Munro, *Nature* **438**, 597 (2005).
6. R. Jahn, T. Lang, T. C. Sudhof, *Cell* **112**, 519 (2003).
7. J. S. Bonifacino, B. S. Glick, *Cell* **116**, 153 (2004).
8. M. Zerial, H. McBride, *Nat. Rev. Mol. Cell Biol.* **2**, 107 (2001).
9. F. R. Maxfield, T. E. McGraw, *Nat. Rev. Mol. Cell Biol.* **5**, 121 (2004).
10. S. Urbe, L. A. Huber, M. Zerial, S. A. Tooze, R. G. Parton, *FEBS Lett.* **334**, 175 (1993).
11. W. Chen, Y. Feng, D. Chen, A. Wandinger-Ness, *Mol. Biol. Cell* **9**, 3241 (1998).
12. G. Emery *et al.*, *Cell* **122**, 763 (2005).
13. S. Wu, S. Q. Mehta, F. Pichaud, H. J. Bellen, F. A. Quiocho, *Nat. Struct. Mol. Biol.* **12**, 879 (2005).
14. R. Prekeris, J. Klumperman, R. H. Scheller, *Mol. Cell* **6**, 1437 (2000).
15. M. Shirane, K. I. Nakayama, *Nat. Cell Biol.* **5**, 28 (2003).
16. J. R. Junutula *et al.*, *J. Biol. Chem.* **279**, 33430 (2004).
17. S. E. Kaiser *et al.*, *Structure* **13**, 1035 (2005).
18. D. J. Gillooly, A. Simonsen, H. Stenmark, *Biochem. J.* **355**, 249 (2001).
19. Single-letter abbreviations for the amino acid residues are as follows: A, Ala; C, Cys; D, Asp; E, Glu; F, Phe; G, Gly; H, His; I, Ile; K, Lys; L, Leu; M, Met; N, Asn; P, Pro; Q, Gln; R, Arg; S, Ser; T, Thr; V, Val; W, Trp; and Y, Tyr.
20. I. Schalk *et al.*, *Nature* **381**, 42 (1996).
21. Y. An *et al.*, *Structure* **11**, 347 (2003).
22. O. Ullrich, S. Reinsch, S. Urbe, M. Zerial, R. G. Parton, *J. Cell Biol.* **135**, 913 (1996).
23. S. Pasqualato *et al.*, *J. Biol. Chem.* **279**, 11480 (2004).
24. C. J. Marshall, *Cell* **80**, 179 (1995).
25. B. Sampo, S. Kaech, S. Kunz, G. Banker, *Neuron* **37**, 611 (2003).
26. D. Wisco *et al.*, *J. Cell Biol.* **162**, 1317 (2003).
27. E. Anderson *et al.*, *J. Cell Biol.* **170**, 595 (2005).
28. A. U. Mannan *et al.*, *Am. J. Hum. Genet.* **79**, 351 (2006).


29. We thank T. Takenawa, M. Takeichi, H. Togashi, Y. Takai, A. Kikuchi, A. Nakano, K. Hanada, H. Sumimoto, Y. Fukui, K. Mihara, Y. Fujiki, M. Hirata, T. Natsume, T. Sasaki, T. Nishi, M. Kohjima, R. Takeya, T. Uemura, and Y. Gotoh

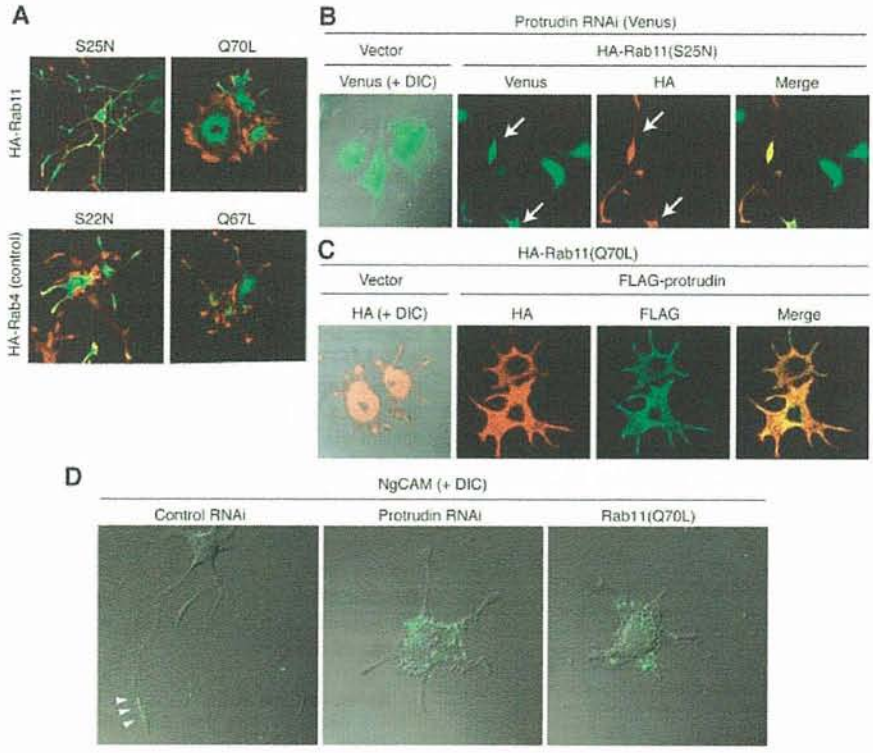


**Fig. 4.** Protrudin induces directional membrane extension through regulation of vesicular traffic. **(A)** PC12 cells expressing HA-Rab11 (S25N or Q70L) or HA-Rab4 (S22N or Q67L) were stimulated with NGF and stained with anti-HA (green) and phalloidin (red). **(B)** PC12 cells transfected with a vector encoding both protrudin shRNA and Venus (green) were also transfected with a HA-Rab11(S25N) vector, incubated with NGF, and stained with anti-HA (red). Arrows indicate cells expressing both Venus (protrudin shRNA) and HA-Rab11(S25N). **(C)** PC12 cells were transfected with HA-Rab11(Q70L) and FLAG-protrudin, stimulated with NGF, and stained with anti-HA (red) and anti-FLAG (green). **(D)** PC12 cells transiently infected with a retrovirus encoding chicken NgCAM were transfected with control or protrudin shRNAs or with Rab11(Q70L). The surface expression of NgCAM was examined by immunostaining with anti-NgCAM (green) without cell permeabilization. Arrowheads indicate the prominent distribution of NgCAM on a neurite.

for discussion; M. Sasaki for electron microscopy; E. Nishida for MEK1 cDNAs; A. Miyawaki for Venus cDNA; P. Sonderegger and B. Winckler for NgCAM cDNA; T. Chano for the pCL-Ampho vector; N. Tanaka for PC12 cells; N. Nishimura, R. Mitsuyasu, F. Matsuzaki, K. Azuma, and K. Oyamada for technical assistance; and M. Kimura and A. Ohta for help in preparation of the manuscript. This work was supported by funds from JST to M.S. and K.I.N.

**Supporting Online Material**
www.sciencemag.org/cgi/content/full/314/5800/818/DC1
Materials and Methods
Figs. S1 to S8
Movies S1 and S2

17 August 2006; accepted 21 September 2006
10.1126/science.1134027

# Where Water Is Oxidized to Dioxygen: Structure of the Photosynthetic $Mn_4Ca$ Cluster

**Junko Yano,[1,2]* Jan Kern,[3]* Kenneth Sauer,[1,2] Matthew J. Latimer,[4] Yulia Pushkar,[1,2] Jacek Biesiadka,[5] Bernhard Loll,[5]† Wolfram Saenger,[5] Johannes Messinger,[6]‡ Athina Zouni,[3]‡ Vittal K. Yachandra[1]‡**

The oxidation of water to dioxygen is catalyzed within photosystem II (PSII) by a $Mn_4Ca$ cluster, the structure of which remains elusive. Polarized extended x-ray absorption fine structure (EXAFS) measurements on PSII single crystals constrain the $Mn_4Ca$ cluster geometry to a set of three similar high-resolution structures. Combining polarized EXAFS and x-ray diffraction data, the cluster was placed within PSII, taking into account the overall trend of the electron density of the metal site and the putative ligands. The structure of the cluster from the present study is unlike either the 3.0 or 3.5 angstrom–resolution x-ray structures or other previously proposed models.

Oxygen, which makes up about 20% of Earth's atmosphere, comes mostly from photosynthesis that occurs in cyanobacteria, green algae, and higher plants (*1*). These organisms have within photosystem II (PSII) an oxygen-evolving complex (OEC), in which the energy of sunlight is used to oxidize water to molecular oxygen. The heart of the OEC is a cluster of four Mn atoms and one Ca atom ($Mn_4Ca$) connected by mono-μ-oxo, di-μ-oxo, and/or hydroxo bridges. The specific protein environment and one chloride ion are also essential for the water-splitting activity (*1*). During the oxidation of water, the OEC cycles through five different oxidation states, which are known as $S_i$ states (where $i$ ranges from 0 to 4), that couple the one-electron photochemistry of the PSII reaction center with the four-electron chemistry of water oxidation (*2*).

The structure of the $Mn_4Ca$ cluster and its role in the mechanism of water oxidation have been investigated with the use of spectroscopic methods (*1*), especially electron paramagnetic resonance and electron nuclear double-resonance spectroscopy (*3*–*9*), x-ray spectroscopy (*10*), and Fourier transform infrared (FTIR) spec-

[1]Melvin Calvin Laboratory, Physical Biosciences Division, Lawrence Berkeley National Laboratory, Berkeley, CA 94720, USA. [2]Department of Chemistry, University of California, Berkeley, CA 94720, USA. [3]Max-Volmer-Laboratorium für Biophysikalische Chemie, Technische Universität, Strasse des 17 Juni 135, D-10623 Berlin, Germany. [4]Stanford Synchrotron Radiation Laboratory, 2575 Sand Hill Road, Menlo Park, CA 94305, USA. [5]Institut für Chemie und Biochemie/Kristallographie, Freie Universität, Takustrasse 6, D-14195 Berlin, Germany. [6]Max-Planck-Institut für Bioanorganische Chemie, Stiftstrasse 34–36, D-45470 Mülheim an der Ruhr, Germany.

*These authors contributed equally to this work.
†Present address: Max-Planck-Institut für Medizinische Forschung, Abteilung für Biomolekulare Mechanismen, Jahnstrasse 29, D-69120 Heidelberg, Germany.
‡To whom correspondence should be addressed. E-mail: messinger@mpi-muelheim.mpg.de (J.M.); zouni@phosis1.chem.tu-berlin.de (A.Z.); vkyachandra@lbl.gov (V.K.Y.)

Available online at www.sciencedirect.com
ScienceDirect
Biochemical and Biophysical Research Communications 350 (2006) 114–119
BBRC
www.elsevier.com/locate/ybbrc

# Expression of mouse Fbxw7 isoforms is regulated in a cell cycle- or p53-dependent manner

Akinobu Matsumoto, Ichiro Onoyama, Keiichi I. Nakayama *

*Department of Molecular and Cellular Biology, Medical Institute of Bioregulation, Kyushu University, 3-1-1 Maidashi, Higashi-ku, Fukuoka, Fukuoka 812-8582, Japan*
*CREST, Japan Science and Technology Agency, 4-1-8 Honcho, Kawaguchi, Saitama 332-0012, Japan*

Received 22 August 2006
Available online 12 September 2006

**Abstract**

Fbxw7 is the F-box protein component of an SCF-type ubiquitin ligase that contributes to the ubiquitin-dependent degradation of cell cycle activators and oncoproteins. Three isoforms (α, β, and γ) of Fbxw7 are produced from mRNAs with distinct 5′ exons. We have now investigated regulation of *Fbxw7* expression in mouse tissues. Fbxw7α mRNA was present in all tissues examined, whereas Fbxw7β mRNA was detected only in brain and testis, and Fbxw7γ mRNA in heart and skeletal muscle. The amount of Fbxw7α mRNA was high during quiescence ($G_0$ phase) in mouse embryonic fibroblasts (MEFs) and T cells, but it decreased markedly as these cells entered the cell cycle. The abundance of Fbxw7α mRNA was unaffected by cell irradiation or p53 status. In contrast, X-irradiation increased the amount of Fbxw7β mRNA in wild-type MEFs but not in those from p53-deficient mice, suggesting that radiation-induced up-regulation of p53 leads to production of Fbxw7β mRNA. Our results thus indicate that expression of Fbxw7 isoforms is differentially regulated in a cell cycle- or p53-dependent manner.


*Keywords:* Ubiquitin; SCF complex; F-box protein; Isoform, p53; Cancer; Cell cycle

The abundance of cyclins, cyclin-dependent kinase inhibitors, and many other regulators of the cell cycle is controlled by the ubiquitin–proteasome system. Various alterations in the ubiquitylation of cell cycle regulators are implicated in the etiology of many human malignancies [1]. Down-regulation of protein abundance by the ubiquitin–proteasome system occurs in two distinct steps [2]: the covalent attachment of multiple ubiquitin molecules to the protein substrate, and degradation of the polyubiquitylated protein by the 26S proteasome complex. The first of these steps is mediated by at least three enzymes: a ubiquitin-activating enzyme (E1), a ubiquitin-conjugating enzyme (E2), and a ubiquitin ligase (E3). Two major classes of E3s, the Skp1–Cul1–F-box protein (SCF) complex and the anaphase-promoting complex or cyclosome (APC/C), play a central role in cell cycle regulation [1]. The SCF complex consists of common subunits (Skp1, Cul1, Rbx1) and a variable substrate-recognition subunit (F-box protein). Three F-box protein components of the SCF complex—S phase kinase-associated protein 2 (Skp2), F-box and WD-40 domain protein 7 (Fbxw7), and β-transducin repeat-containing protein (β-TRCP)—have been thought to contribute primarily to cell cycle regulation.

Fbxw7 is the F-box protein of an SCF complex that targets several oncoproteins, including cyclin E, c-Myc, Notch, and c-Jun, for degradation [1]. Fbxw7 was first discovered by genetic screening as a negative regulator of the LIN-12 (Notch) signaling pathway in *Caenorhabditis elegans* [3]. We and others have generated mice that are deficient in Fbxw7 and found that the homozygous mutant embryos die in utero at embryonic day 10.5 manifesting marked abnormalities in vascular development [4,5]. Notch4 accumulates in *Fbxw7*$^{-/-}$ embryos, resulting in

* Corresponding author. Fax: +81 92 642 6819.
*E-mail address:* nakayak1@bioreg.kyushu-u.ac.jp (K.I. Nakayama).

0006-291X/$ - see front matter © 2006 Elsevier Inc. All rights reserved.
doi:10.1016/j.bbrc.2006.09.003

increased expression of Hey1, a transcriptional repressor that acts downstream of Notch and is implicated in vascular development. These observations suggest that Fbxw7 plays an essential role in mammalian vascular development by regulating Notch stability during embryogenesis.

Given that Fbxw7 is responsible for degradation of the above-mentioned oncoproteins, it is thought to function as a tumor suppressor. Indeed, mutations in *FBXW7* have been identified in human ovarian [6], breast [7,8], endometrial [9,10], and colorectal [11] cancers. The loss of Fbxw7 in cultured cells also results in genetic instability [11]. In addition, *Fbxw7*$^{+/-}$ mice exhibit an increased susceptibility to radiation-induced tumorigenesis even though most tumors retain and express the wild-type allele, indicating that *Fbxw7* is a haploinsufficient tumor suppressor gene [12].

The *FBXW7* locus maps to human chromosomal region 4q32, which is frequently deleted in a wide range of human tumor types [13]. This locus encodes three protein isoforms (Fbxw7α, Fbxw7β, Fbxw7γ) [7,9,14,15], each of which is translated from an mRNA with a unique 5′ exon and 10 shared exons. Each isoform of Fbxw7 exhibits a distinct subcellular distribution: Fbxw7α is localized in the nucleus, Fbxw7β shows a cytoplasmic distribution suggestive of localization to the endoplasmic reticulum (ER) and Golgi apparatus, and Fbxw7γ is predominantly nucleolar [16,17]. Northern blot analysis of human tissues revealed that Fbxw7α mRNA is widely distributed, whereas Fbxw7β/γ mRNA (the probe did not distinguish between the two transcripts) is restricted to brain, heart, and skeletal muscle [9]. Expression of Fbxw7β was shown to be up-regulated by p53, and a potential p53 binding site is present in exon 1b of human *FBXW7* [18]. However, the regulation of Fbxw7α/γ expression has remained uncharacterized. Furthermore, most studies of Fbxw7β expression have been performed with cultured human cell lines, and the results therefore require verification in other species with primary cultured cells.

With the use of tissues and primary cultured cells, including embryonic fibroblasts (MEFs) and freshly isolated T cells, from wild-type or *p53*$^{-/-}$ mice, we have now shown that Fbxw7β and Fbxw7γ mRNAs exhibit different tissue and cell distributions. Furthermore, we found that Fbxw7α mRNA is abundant in quiescent NIH 3T3 cells and T cells but is down-regulated on entry of these cells into the cell cycle. Whereas the level of Fbxw7α mRNA in MEFs does not appear to be affected by p53 status, that of Fbxw7β mRNA is regulated in a p53-dependent manner. These observations suggest that the spatiotemporal control of *Fbxw7* expression in mice is mediated in an isoform-specific manner.

## Materials and methods

*Cells.* Wild-type or *p53*$^{-/-}$ MEFs as well as freshly isolated lymphocytes were prepared as described previously [19,20]. For radiation treatment, cells were exposed to 0, 2, 4, or 8 Gy of ionizing radiation and then incubated at 37 °C for 4 h (MEFs) or 2 h (thymocytes). Splenic T cells were isolated to a purity of ~90% with the use of a T Cell Enrich column (R&D Systems); they were stimulated for the indicated times with plate-bound antibodies to (anti-) CD3ε (coated at 5 μg/ml; 145-2C11, BD Bioscience Pharmingen) in 96-well plates.

*Quantitation of mRNA by RT-PCR.* Total RNA was extracted from cells by the guanidinium thiocyanate–phenol-chloroform method, purified, and subjected (1 μg) to reverse transcription (RT) with random hexanucleotide primers (ReverTra Ace α, Toyobo). The resulting cDNA was then subjected to quantitative polymerase chain reaction (PCR) analysis with 1× SYBR Green PCR master mix (Applied Biosystems) and 200 nM gene-specific primers. Assays were performed in triplicate with an ABI Prism 7700 sequence detector (Applied Biosystems). The amplification protocol comprised initial incubation at 60 °C for 31 s and 95 °C for 5 s followed by 40 cycles. The sequences of the various primers (sense and antisense, respectively) were 5′-GCCTAAGATGAGCGCAAGTTG-3′ and 5′-TACTAGGCAGATGGCCACAGG-3′ for hypoxanthine phosphoribosyltransferase (HPRT), 5′-CTCACCAGCTCTCCTCTCCATT-3′ and 5′-GCTGAACATGGTACAAGGCCA-3′ for Fbxw7α, 5′-TTGTCA GAGACTGCCAAGCAG-3′ and 5′-GACTTTGCATGGTTTCTTTC CC-3′ for Fbxw7β, 5′-AACCATGGCTTGGTTCCTGTTG-3′ and 5′-CAGAACCATGGTCCAACTTTC-3′ for Fbxw7γ, and 5′-TGTCTG AGCGGCCTGAAGATTC-3′ and 5′-GCAGAAGACCAATCTGCG CTTG-3′ for p21. Each reaction was performed concurrently on the same plate with an HPRT control, and the results were normalized relative to HPRT mRNA abundance.

*Flow cytometry.* Fluorescein isothiocyanate (FITC)-conjugated anti-BrdU, which was from BD Bioscience Pharmingen, was used for flow cytometry. All analyses were performed with FACSCalibur instrument (Becton–Dickinson). For cell cycle analysis, purified splenic T cells or NIH 3T3 cells were exposed to 10 μM bromodeoxyuridine (BrdU) during the last 1 h of incubation, washed with phosphate-buffered saline, fixed in 70% ethanol at 4 °C, and incubated for 30 min at room temperature with 2 M HCl containing 0.5% Triton X-100. After neutralization with 0.1 M sodium tetraborate (pH 8.5), the cells were washed with phosphate-buffered saline containing 1% bovine serum albumin and 0.5% Tween 20, stained with FITC-conjugated anti-BrdU, washed again, stained with propidium iodide (PI), and then analyzed by flow cytometry.

*Statistical analysis.* Quantitative data are expressed as means ± SD and were analyzed by Student's *t* test. A $P$ value of $<0.05$ was considered statistically significant.

## Results

### *Tissue distribution of Fbxw7 isoform mRNAs in mice*

We investigated the distribution of Fbxw7 isoform mRNAs in mouse tissues by semiquantitative RT-PCR analysis with sets of specific primers corresponding to the distinct 5′ exon of each mRNA. Fbxw7α mRNA was detected in all tissues examined (Fig. 1). In contrast, Fbxw7β and Fbxw7γ mRNAs were found to be restricted to brain and testis, and to heart and skeletal muscle, respectively. Fbxw7α and Fbxw7β mRNAs, but not Fbxw7γ mRNA, were also detected in MEFs. In the following experiments, we attempted to characterize the regulation of Fbxw7α and Fbxw7β mRNA abundance in cultured mouse cells.

### *Fbxw7α mRNA is enriched in quiescent cells*

Given that Fbxw7 is thought to contribute to the ubiquitin-dependent degradation of cell cycle activators such as

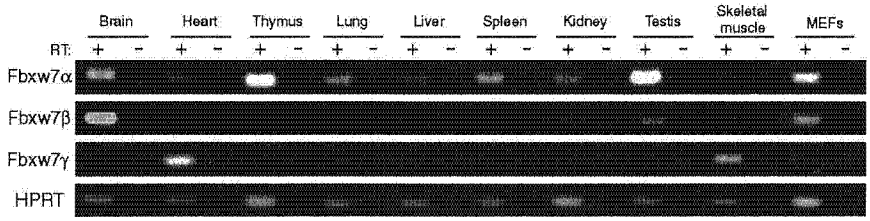


Fig. 1. Distribution of Fbxw7 isoform mRNAs in mouse tissues. The amounts of Fbxw7α, Fbxw7β, and Fbxw7γ mRNAs in the indicated tissues and cells were determined by semiquantitative RT-PCR analysis. RT (+) and RT (−) indicate reactions performed with or without reverse transcriptase, respectively.

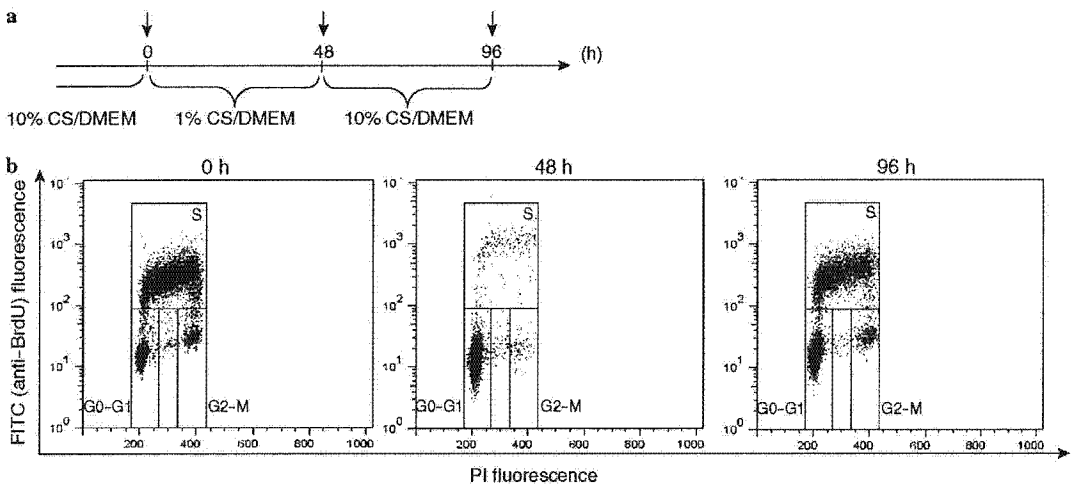


| Time (h) | G0-G1 (%) | S (%) | G2-M (%) |
|---|---|---|---|
| 0 | 24.1 | 68.4 | 6.6 |
| 48 | 95.1 | 2.7 | 1.2 |
| 96 | 49.6 | 45.3 | 4.5 |

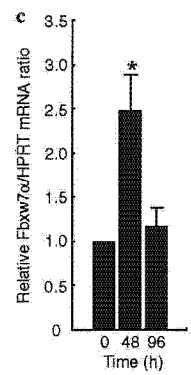


Fig. 2. Cell cycle-dependent regulation of Fbxw7α mRNA in NIH 3T3 cells. (a) Protocol for induction of arrest and subsequent reactivation of the cell cycle. Cells cultured in Dulbeccos's modified Eagle's medium (DMEM) supplemented with 10% calf serum (CS) were incubated for 48 h in DMEM containing 1% CS and then for 48 h in DMEM containing 10% CS. They were harvested at time 0, 48, and 96 h as indicated. (b) Flow cytometric analysis of cell cycle status. The percentages of cells in $G_0$ or $G_1$, in S, and in $G_2$ or M phases of the cell cycle at each time point are indicated. (c) RT and real-time PCR analysis of Fbxw7α mRNA at the indicated time points. Data are means ± SD of triplicates from a representative experiment. $^*P < 0.01$ versus value for time 0.

cyclin E, c-Myc, and c-Jun, we hypothesized that Fbxw7 might be expressed specifically in quiescent cells. To test this hypothesis, we induced quiescence in NIH 3T3 cells by depriving them of serum for 48 h and then examined the level of Fbxw7α mRNA by RT and real-time PCR analysis (Fig. 2a). Cell cycle status was monitored by flow cytometric analysis (Fig. 2b). The amount of Fbxw7α mRNA was increased in response to serum deprivation, and it subsequently returned to its original level on stimulation of the cells to re-enter the cell cycle by replenishment of serum (Fig. 2c).

We also measured the level of Fbxw7α mRNA in freshly isolated splenic T cells. Flow cytometric analysis revealed that only a small proportion (0.8%) of these cells was in

S phase, indicative of cell cycle arrest (Fig. 3a). Mitogenic stimulation with anti-CD3ε increased the proportion of cells in S phase in a time-dependent manner. The amount of Fbxw7α mRNA was significantly reduced 24 h after the initiation of stimulation with anti-CD3ε (Fig. 3b), when 5.2% of the cells had entered S phase (Fig. 3a). The decrease in the level of Fbxw7α mRNA was more pronounced at 48 h, when 45.4% of cells were in S phase. Together, these results showed that Fbxw7α mRNA is most abundant in quiescent cells and undergoes down-regulation as cells enter the cell cycle. The abundance of Fbxw7β and Fbxw7γ mRNAs is too low to be detected in NIH 3T3 cells and splenocytes by RT-PCR.

### *Genotoxic stress up-regulates Fbxw7β mRNA in a p53-dependent manner*

We exposed MEFs or mouse thymocytes to 0, 2, 4, or 8 Gy of X-radiation and then examined the abundance of Fbxw7α and Fbxw7β mRNAs by quantitative RT-PCR analysis at 4 h (MEFs) or 2 h (thymocytes) thereafter. Fbxw7α mRNA was detected in both MEFs and thymocytes, but its abundance in these cells was not affected by X-radiation (Fig. 4a). In contrast, Fbxw7β mRNA was detected only in MEFs, and its abundance in these cells was increased by X-radiation in a dose-dependent manner (Fig. 4b). As a positive control, p21 mRNA was shown to be up-regulated by X-radiation in both cell types, although its abundance was markedly greater in MEFs than in thymocytes (Fig. 4c).

To examine whether the up-regulation of Fbxw7β mRNA by X-radiation in MEFs is mediated by p53, we compared the effects of irradiation between MEFs derived from wild-type or *p53*$^{-/-}$ mice. The amount of Fbxw7α mRNA in *p53*$^{-/-}$ MEFs was similar to that in the wild-type cells and was not affected by X-radiation (Fig. 4a). In contrast, the basal level of Fbxw7β mRNA in *p53*$^{-/-}$ MEFs was greatly reduced compared with that in wild-type MEFs, and it was not increased in response to X-irradiation (Fig. 4b). Similar results were obtained with p21 mRNA (Fig. 4c), the gene for which is p53 inducible. Fbxw7γ mRNA was not detected in MEFs by RT-PCR. Our data suggest that the production of Fbxw7β mRNA, but not that of Fbxw7α mRNA, is activated by p53.

## Discussion

Fbxw7 has been implicated as a key regulator of the cell cycle and an oncosuppressor protein, given that most proteins targeted by Fbxw7 for degradation are cell cycle

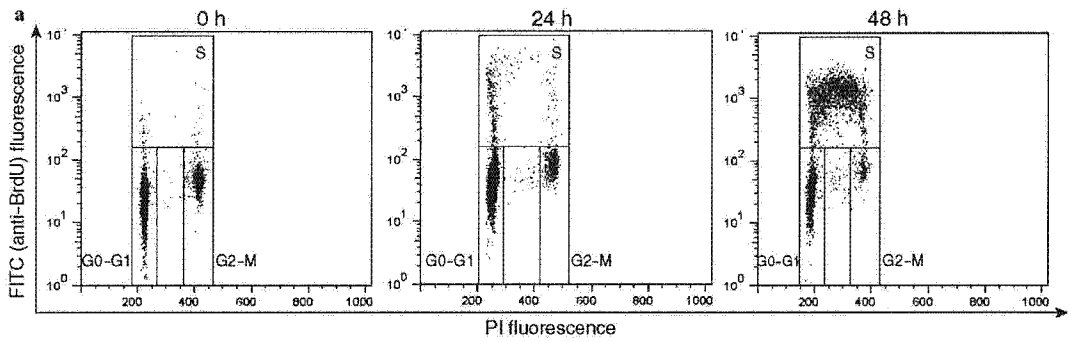


| Time (h) | G0-G1 (%) | S (%) | G2-M (%) |
|---|---|---|---|
| 0 | 86.0 | 0.8 | 12.9 |
| 24 | 85.6 | 5.2 | 8.5 |
| 48 | 49.6 | 45.4 | 3.9 |

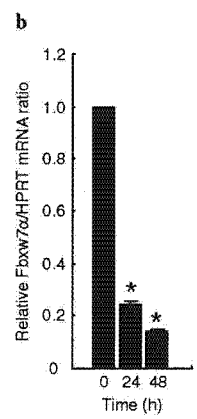


Fig. 3. Down-regulation of Fbxw7α mRNA on entry of splenic T cells into the cell cycle. (a) Splenic T cells were stimulated with anti-CD3ε in RPMI-1640 supplemented with 10% fetal calf serum for 0, 24, or 48 h, at which times cell cycle status was determined by flow cytometry. The percentages of cells in $G_0$–$G_1$, S, and $G_2$–M phases of the cell cycle at each time point are shown. (b) RT and real-time PCR analysis of Fbxw7α mRNA at the indicated time points. $^*P < 0.01$ versus value for time 0.

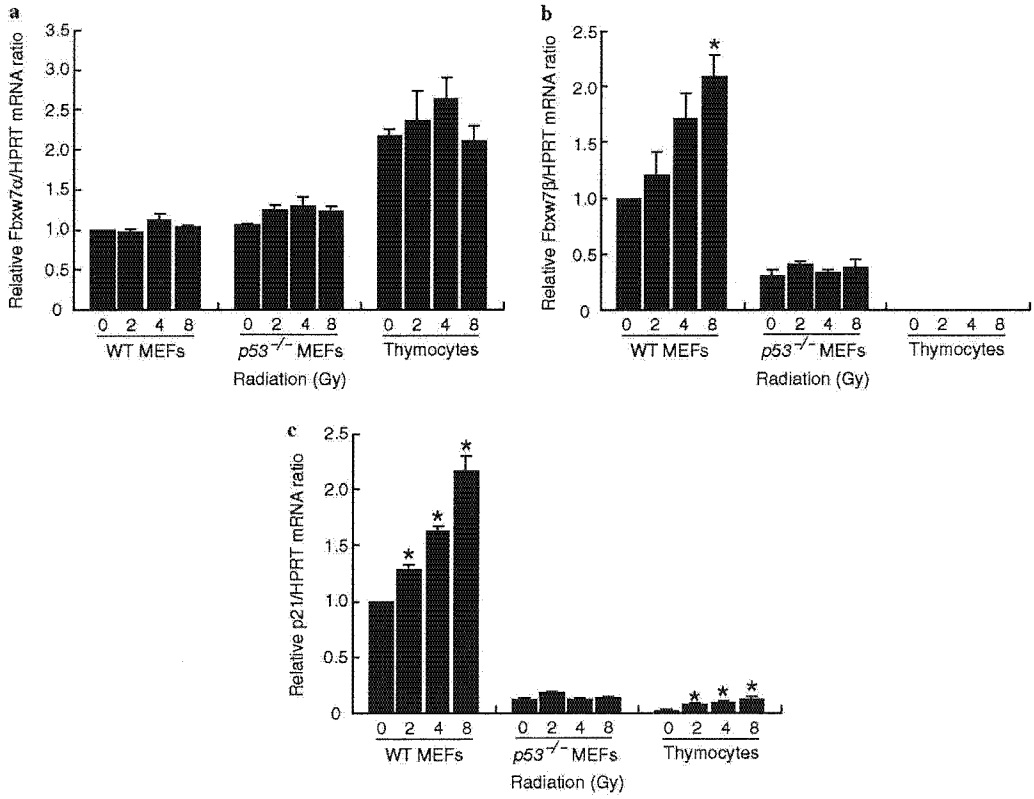


Fig. 4. Up-regulation of Fbxw7β mRNA by X-radiation in a p53-dependent manner. Wild-type (WT) or $p53^{-/-}$ MEFs as well as wild-type thymocytes were exposed to 0, 2, 4, or 8 Gy of ionizing radiation and then incubated for 4 h (MEFs) or 2 h (thymocytes) at 37 °C in DMEM (MEFs) or RPMI-1640 (thymocytes) supplemented with 10% fetal calf serum. The abundance of Fbxw7α (a), Fbxw7β (b), and p21 (c) mRNAs was determined by RT and real-time PCR analysis. Data for each mRNA are expressed relative to the corresponding value for nonirradiated wild-type MEFs. $^{*}P < 0.01$ versus value for corresponding nonirradiated cells.

activators, such as cyclin E, c-Myc, and c-Jun [1]. Consistent with this notion, mutations in *FBXW7* have been detected in certain human malignancies [6–11,15]. Like cyclin E, c-Myc, and c-Jun, Fbxw7α is localized to the nucleoplasm. Our results now indicate that the abundance of Fbxw7α mRNA is highest in quiescent cells and decreases as cells enter the cell cycle. This expression pattern is consistent with an antiproliferative action of Fbxw7α. The mechanism underlying this cell cycle-dependent regulation of Fbxw7α expression remains to be determined.

Fbxw7β is localized to the ER membrane in the cytoplasm [16,17], a localization likely mediated by a putative transmembrane domain that is present near the $NH_2$-terminus and encoded by the β isoform-specific 5′ exon [14]. Although cytoplasmic cyclin E has been suggested as a target of Fbxw7β [17], the bona fide targets and functions of Fbxw7β remain unknown. In contrast, Fbxw7γ, which is localized to the nucleolus, was shown to contribute to control both of the amount of c-Myc in the nucleolus and of cell size [16]. The tissue distribution patterns of Fbxw7β and Fbxw7γ may provide insight into their functions. Fbxw7β mRNA is largely restricted to the brain, suggesting that the targets of Fbxw7β might be ER-associated proteins in neurons. Parkin, mutations in the gene for which are responsible for an autosomal recessive, early onset form of Parkinson's disease, has been shown to interact with Fbxw7 [21]. Among potential targets of parkin, the Pael receptor is an ER-resident protein and is ubiquitylated by the ER-associated protein degradation pathway [22,23]. These observations thus implicate Fbxw7β in degradation of the Pael receptor. Fbxw7γ mRNA is largely restricted to muscle tissue, including the heart and skeletal muscle. Given the role of Fbxw7γ in regulation both of the nucleolar level of c-Myc and of cell size and that muscle fibers are large compared with other cell types, Fbxw7γ might contribute to muscle differentiation through regulation of c-Myc-dependent cell growth.

We previously identified mouse *Fbxw7* as a p53-dependent tumor suppressor gene with the use of a mammalian genetic screen for p53-dependent genes involved in tumorigenesis [12]. $Fbxw7^{+/-}$ mice manifest an increased susceptibility to radiation-induced tumorigenesis, although most of the induced tumors retain and express the wild-type allele. Loss of Fbxw7 also alters the spectrum of tumors that develop in p53-deficient mice to include those of epithelial tissues in the lung, liver, and ovary. Radiation-

induced lymphomas in $p53^{+/-}$ mice, but not those in $p53^{-/-}$ mice, also show frequent deletion or mutation of *Fbxw7*. We have now shown that Fbxw7α mRNA is present in T cells, but that its abundance in these cells appears to be independent of p53. In contrast, the amount of Fbxw7β mRNA in MEFs was shown to be controlled by p53, but this transcript was not detected in thymocytes. These results suggest that the total amount of Fbxw7 isoforms is unlikely to be reduced more in $Fbxw7^{+/-};p53^{+/-}$ T cells than in $Fbxw7^{+/-}$ T cells. It thus remains to be determined why a decrease in *Fbxw7* expression results in tumorigenesis in a p53-dependent manner.

## Acknowledgments

We thank Masaaki Nishiyama for p21 primers for quantitative RT-PCR; Koji Oyamada and Naoko Nishimura for technical assistance; Ryosuke Tsunematsu, Takamichi Sato, Etsuo Susaki, Toru Saiga, Tadashi Nakagawa, and other members of our laboratory for comments on the manuscript; and Akane Ohta and Mihoko Kimura for help in preparation of the manuscript.

## References

[1] K.I. Nakayama, K. Nakayama, Ubiquitin ligases: cell-cycle control and cancer, Nat. Rev. Cancer 6 (2006) 369–381.
[2] A. Hershko, A. Ciechanover, The ubiquitin system, Annu. Rev. Biochem. 67 (1998) 425–479.
[3] E.J. Hubbard, G. Wu, J. Kitajewski, I. Greenwald, sel-10, a negative regulator of lin-12 activity in *Caenorhabditis elegans*, encodes a member of the CDC4 family of proteins, Genes Dev. 11 (1997) 3182–3193.
[4] R. Tsunematsu, K. Nakayama, Y. Oike, M. Nishiyama, N. Ishida, S. Hatakeyama, Y. Bessho, R. Kageyama, T. Suda, K.I. Nakayama, Mouse Fbw7/Sel-10/Cdc4 is required for notch degradation during vascular development, J. Biol. Chem. 279 (2004) 9417–9423.
[5] M.T. Tetzlaff, W. Yu, M. Li, P. Zhang, M. Finegold, K. Mahon, J.W. Harper, R.J. Schwartz, S.J. Elledge, Defective cardiovascular development and elevated cyclin E and Notch proteins in mice lacking the Fbw7 F-box protein, Proc. Natl. Acad. Sci. USA 101 (2004) 3338–3345.
[6] E.L. Kwak, K.H. Moberg, D.C. Wahrer, J.E. Quinn, P.M. Gilmore, C.A. Graham, I.K. Hariharan, D.P. Harkin, D.A. Haber, D.W. Bell, Infrequent mutations of Archipelago (hAGO, hCDC4, Fbw7) in primary ovarian cancer, Gynecol. Oncol. 98 (2005) 124–128.
[7] H. Strohmaier, C.H. Spruck, P. Kaiser, K.A. Won, O. Sangfelt, S.I. Reed, Human F-box protein hCdc4 targets cyclin E for proteolysis and is mutated in a breast cancer cell line, Nature 413 (2001) 316–322.
[8] S. Ekholm-Reed, C.H. Spruck, O. Sangfelt, F. van Drogen, E. Mueller-Holzner, M. Widschwendter, A. Zetterberg, S.I. Reed, Mutation of hCDC4 leads to cell cycle deregulation of cyclin E in cancer, Cancer Res. 64 (2004) 795–800.
[9] C.H. Spruck, H. Strohmaier, O. Sangfelt, H.M. Muller, M. Hubalek, E. Muller-Holzner, C. Marth, M. Widschwendter, S.I. Reed, hCDC4 gene mutations in endometrial cancer, Cancer Res. 62 (2002) 4535–4539.
[10] R. Cassia, G. Moreno-Bueno, S. Rodriguez-Perales, D. Hardisson, J.C. Cigudosa, J. Palacios, Cyclin E gene (CCNE) amplification and hCDC4 mutations in endometrial carcinoma, J. Pathol. 201 (2003) 589–595.
[11] H. Rajagopalan, P.V. Jallepalli, C. Rago, V.E. Velculescu, K.W. Kinzler, B. Vogelstein, C. Lengauer, Inactivation of hCDC4 can cause chromosomal instability, Nature 428 (2004) 77–81.
[12] J.H. Mao, J. Perez-Losada, D. Wu, R. Delrosario, R. Tsunematsu, K.I. Nakayama, K. Brown, S. Bryson, A. Balmain, Fbxw7/Cdc4 is a p53-dependent, haploinsufficient tumour suppressor gene, Nature 432 (2004) 775–779.
[13] S. Knuutila, Y. Aalto, K. Autio, A.M. Bjorkqvist, W. El-Rifai, S. Hemmer, T. Huhta, E. Kettunen, S. Kiuru-Kuhlefelt, M.L. Larramendy, T. Lushnikova, O. Monni, H. Pere, J. Tapper, M. Tarkkanen, A. Varis, V.M. Wasenius, M. Wolf, Y. Zhu, DNA copy number losses in human neoplasms, Am. J. Pathol. 155 (1999) 683–694.
[14] D.M. Koepp, L.K. Schaefer, X. Ye, K. Keyomarsi, C. Chu, J.W. Harper, S.J. Elledge, Phosphorylation-dependent ubiquitination of cyclin E by the $SCF^{Fbw7}$ubiquitin ligase, Science 294 (2001) 173–177.
[15] K.H. Moberg, D.W. Bell, D.C. Wahrer, D.A. Haber, I.K. Hariharan, Archipelago regulates Cyclin E levels in Drosophila and is mutated in human cancer cell lines, Nature 413 (2001) 311–316.
[16] M. Welcker, A. Orian, J.E. Grim, R.N. Eisenman, B.E. Clurman, A nucleolar isoform of the Fbw7 ubiquitin ligase regulates c-Myc and cell size, Curr. Biol. 14 (2004) 1852–1857.
[17] X. Ye, G. Nalepa, M. Welcker, B.M. Kessler, E. Spooner, J. Qin, S.J. Elledge, B.E. Clurman, J.W. Harper, Recognition of phosphodegron motifs in human cyclin E by the $SCF^{Fbw7}$ubiquitin ligase, J. Biol. Chem. 279 (2004) 50110–50119.
[18] T. Kimura, M. Gotoh, Y. Nakamura, H. Arakawa, hCDC4b, a regulator of cyclin E, as a direct transcriptional target of p53, Cancer Sci. 94 (2003) 431–436.
[19] K. Nakayama, N. Ishida, M. Shirane, A. Inomata, T. Inoue, N. Shishido, I. Horii, D.Y. Loh, K.I. Nakayama, Mice lacking $p27^{Kip1}$ display increased body size, multiple organ hyperplasia, retinal dysplasia, and pituitary tumors, Cell 85 (1996) 707–720.
[20] K. Nakayama, H. Nagahama, Y.A. Minamishima, M. Matsumoto, I. Nakamichi, K. Kitagawa, M. Shirane, R. Tsunematsu, T. Tsukiyama, N. Ishida, M. Kitagawa, K.I. Nakayama, S. Hatakeyama, Targeted disruption of *Skp2* results in accumulation of cyclin E and $p27^{Kip1}$, polyploidy and centrosome overduplication, EMBO J. 19 (2000) 2069–2081.
[21] J.F. Staropoli, C. McDermott, C. Martinat, B. Schulman, E. Demireva, A. Abeliovich, Parkin is a component of an SCF-like ubiquitin ligase complex and protects postmitotic neurons from kainate excitotoxicity, Neuron 37 (2003) 735–749.
[22] Y. Imai, M. Soda, H. Inoue, N. Hattori, Y. Mizuno, R. Takahashi, An unfolded putative transmembrane polypeptide, which can lead to endoplasmic reticulum stress, is a substrate of Parkin, Cell 105 (2001) 891–902.
[23] Y. Imai, M. Soda, S. Hatakeyama, T. Akagi, T. Hashikawa, K.I. Nakayama, R. Takahashi, CHIP is associated with Parkin, a gene responsible for familial Parkinson's disease, and enhances its ubiquitin ligase activity, Mol. Cell 10 (2002) 55–67.

nature
cell biology

# Mitogenic signalling and the p16$^{INK4a}$–Rb pathway cooperate to enforce irreversible cellular senescence

Akiko Takahashi[1], Naoko Ohtani[1], Kimi Yamakoshi[1], Shin-ichi Iida[2], Hidetoshi Tahara[3], Keiko Nakayama[4], Keiichi I. Nakayama[5], Toshinori Ide[6], Hideyuki Saya[2] and Eiji Hara[1,7]

**The p16$^{INK4a}$ cyclin-dependent kinase inhibitor has a key role in establishing stable G1 cell-cycle arrest through activating the retinoblastoma (Rb) tumour suppressor protein pRb[1–5] in cellular senescence. Here, we show that the p16$^{INK4a}$/Rb-pathway also cooperates with mitogenic signals to induce elevated intracellular levels of reactive oxygen species (ROS), thereby activating protein kinase C δ (PKCδ) in human senescent cells. Importantly, once activated by ROS, PKCδ promotes further generation of ROS, thus establishing a positive feedback loop to sustain ROS–PKCδ signalling[6–8]. Sustained activation of ROS–PKCδ signalling irreversibly blocks cytokinesis, at least partly through reducing the level of WARTS (also known as LATS1), a mitotic exit network (MEN) kinase required for cytokinesis[9–11], in human senescent cells. This irreversible cytokinetic block is likely to act as a second barrier to cellular immortalization ensuring stable cell-cycle arrest in human senescent cells. These results uncover an unexpected role for the p16$^{INK4a}$–Rb pathway and provide a new insight into how senescent cell-cycle arrest is enforced in human cells.**

Oncogenic proliferative signals are coupled to a variety of growth inhibitory processes, such as the induction of apoptotic cell death or senescent cell-cycle arrest[1]. Thus, both apoptosis and senescence are thought to act as a safe-guard against neoplasia. Unlike apoptotic cells, senescent cells are viable for long periods of time[2,3]. It is therefore important to clarify how senescent cell-cycle arrest is enforced in human cells[2]. Two well established tumour suppressor gene products, pRb and p53, are known to have key roles in senescent cell-cycle arrest[3–5]. The activities of pRb and p53 are dramatically increased during cellular senescence and inactivation of these proteins in senescent mouse embryonic fibroblasts (MEFs) results in reversal of the senescent phenotype leading to cell-cycle re-entry[12,13], suggesting that pRb and p53 are required not only for the onset of cellular senescence, but also for the maintenance of the senescence programme in murine cells. However, in human cells, once pRb is fully engaged, particularly by its activator, p16$^{INK4a}$, senescent growth arrest becomes irreversible and is no longer revoked by subsequent inactivation of pRb and p53 (refs 2, 14, 15). Interestingly, subsequent inactivation of pRb and p53 enables human senescent cells to reinitiate DNA synthesis, but fails to drive a complete cell cycle, suggesting that these cells may be arrested in G2 or M phase of the cell cycle[14,16]. However, to date, it is largely unknown how senescent cell-cycle arrest is maintained, even after pRb and p53 are subsequently inactivated in human senescent cells.

To delineate the molecular mechanisms of irreversible cell-cycle arrest in human cell senescence, we used SVts8 cells, a conditionally immortalized human fibroblast cell line that express a temperature-sensitive (ts) mutant of simian virus 40 large T antigen and elevated level of the endogenous telomerase[17]. SVts8 cells proliferate indefinitely at the permissive temperature (34 °C; Fig. 1a), because large T antigen binds and inactivates both pRb and p53 proteins (Fig.1b). However, when shifted to the non-permissive temperature (38.5 °C), large T antigen is inactivated and a senescence-like cell-cycle arrest was induced within 5 days (Fig. 1a, b and see Supplementary Information, Fig. S1a). Importantly, once the senescence-like phenotype was induced, subsequent inactivation of pRb and p53 by large T antigen was no longer able to revoke cell-cycle arrest, even though a significant fraction of cells reinitiated DNA synthesis (Fig. 1a–d). These results are consistent with previous data from senescent human primary fibroblasts[14,16], indicating that SVts8 cells are an ideal model system to study irreversible senescent cell-cycle arrest. Interestingly, if Svts8 cells were cultured in low serum (0.2%) medium throughout the incubation at 38.5 °C, a significant fraction of cells reinitiated not only DNA synthesis, but also cell proliferation on shifting the temperature to 34 °C in normal serum (10%) medium (Fig. 1a, c and d). This is not simply because large T antigen was incompletely inactivated in low serum medium at 38.5 °C, as large T antigen was equally dissociated from both pRb and p53, and transcriptional control activities of pRb and p53 were similarly restored at 38.5 °C regardless of serum concentration in culture medium (Fig. 1b and see Supplementary

[1]Institute for Genome Research, University of Tokushima, Tokushima 770-8503, Japan. [2]Graduate School of Medical Science, Kumamoto University, Kumamoto 860-8556, Japan. [3]Hiroshima University School of Medicine, Hiroshima 734-8551, Japan. [4]Graduate School of Medicine, Tohoku University, Sendai 980-8575, Japan. [5]Medical Institute of Bioregulation, Kyushu University, Fukuoka 812-8582, Japan. [6]Faculty of Pharmaceutical Sciences, Hiroshima International University, Kure 737-0112, Japan.
[7]Correspondence should be addressed to E.H. (e-mail: hara@genome.tokushima-u.ac.jp)

Received 22 June 2006; accepted 30 August 2006; published online 8 October 2006; DOI: 10.1038/ncb1491

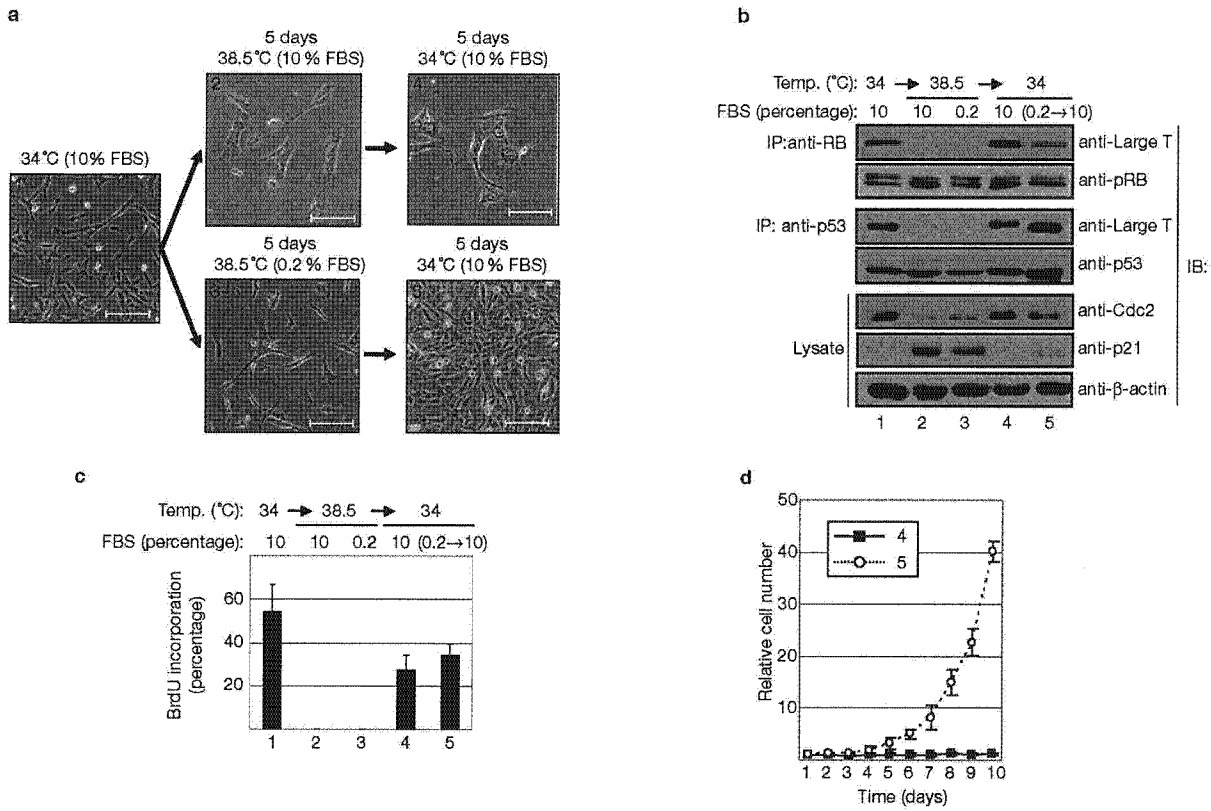


**Figure 1** Mitogenic signals cooperate with pRb and/or p53 to induce irreversible cell-cycle arrest. (**a**) Time line of temperature shift experiments using SVts8 cells. SVts8 cells were cultured in normal serum (10%) medium at 34 °C. Cells were then incubated at 38.5 °C in normal serum medium or in low serum (0.2%) medium for 5 days. These cells were subsequently incubated at 34 °C in normal serum medium for another 5 days. Representative photographs of the cells in the indicated culture conditions are shown. The scale bars represent 200 μm. (**b**) Total cell lysates were prepared at indicated times in **a** (clumn number corresponds to culture condition in Fig. 1a) and were immunoblotted (IB) after immunoprecipitation (IP). The antibodies used are indicated. The total amount of Cdc2, p21 and β-actin were monitored by direct immunoblotting of the cell lysate. (**c**) A BrdU incorporation assay was performed at the times indicated in **a**. The means ± s.d. of three independent experiments are shown. (**d**) SVts8 cells were cultured at 38.5 °C either in normal serum medium (4) or in low serum medium (5) for 5 days. Cells were then cultured at 34 °C in normal serum medium and were subjected to a cell proliferation assay performed in triplicate. The means ± s.d. of three independent experiments are shown.

Information, Fig. S1a). Thus, it seems that pRb and/or p53 may require mitogenic signals to initiate a cascade of molecular events underlying irreversible senescent cell-cycle arrest[18,19].

To understand how mitogenic signalling collaborates with pRb and/or p53 to induce irreversible senescent cell-cycle arrest, we focused on the intracellular levels of ROS because ROS are known to be induced by various mitogenic signals[20] and are implicated in the onset of cellular senescence[21]. Intriguingly, the levels of ROS were significantly increased on shifting the temperature to 38.5 °C in normal serum medium (Fig. 2a) and this level remained high even after pRb and p53 were subsequently inactivated by shifting the temperature to 34 °C in SVts8 cells (Fig. 2a). Importantly, induction of ROS was markedly attenuated if SVts8 cells were cultured in low serum medium throughout the incubation at 38.5 °C (Fig. 2a), suggesting that the increased level of ROS may determine the irreversibility of senescent cell-cycle arrest. To test this hypothesis, production of ROS was inhibited by addition of N-acetyl-cysteine (NAC) throughout the incubation at 38.5 °C in normal serum medium (Fig. 2b). Interestingly, NAC treatment enabled SVts8 cells to reinitiate cell proliferation on shifting the temperature to 34 C in normal serum medium (Fig. 2c). Similar results were also observed when diphenylene iodonium (DPI), an inhibitor of nicotinamide adenine dinucleotide diphoshate (NADPH) oxidase, was used instead of NAC (see Supplementary Information, Fig. S1c, d and e).

PKCδ has an established role in activating NADPH-oxidase through phosphorylating $p47^{phox}$, an essential component of NADPH oxidase[7,8], and the levels of its catalytically active fragment (PKCδ-CF) were shown to be increased during replicative senescence in human diploid fibroblasts (HDFs)[22]. This evidence, in conjunction with previous reports showing that PKCδ acts as a critical downstream mediator of the ROS signalling pathway[7,8,23], led us to hypothesize that once activated by ROS, PKCδ itself activates production of ROS through activating NADPH oxidase, thereby establishing a positive-feedback loop to sustain the levels of ROS, even after pRb and p53 were subsequently inactivated in senescent cells. To explore this possibility, the levels of PKCδ-CF and its kinase activity were measured in SVts8 cells. An intense band with a relative molecular mass of 40,000 ($M_r$ 40K), which corresponds to PKCδ-CF, was observed almost exclusively on restoration of pRb and p53 in normal serum medium in SVts8 cells (Fig. 2d). Importantly, the levels of PKCδ-CF and its kinase activity were even higher when pRb and p53 were

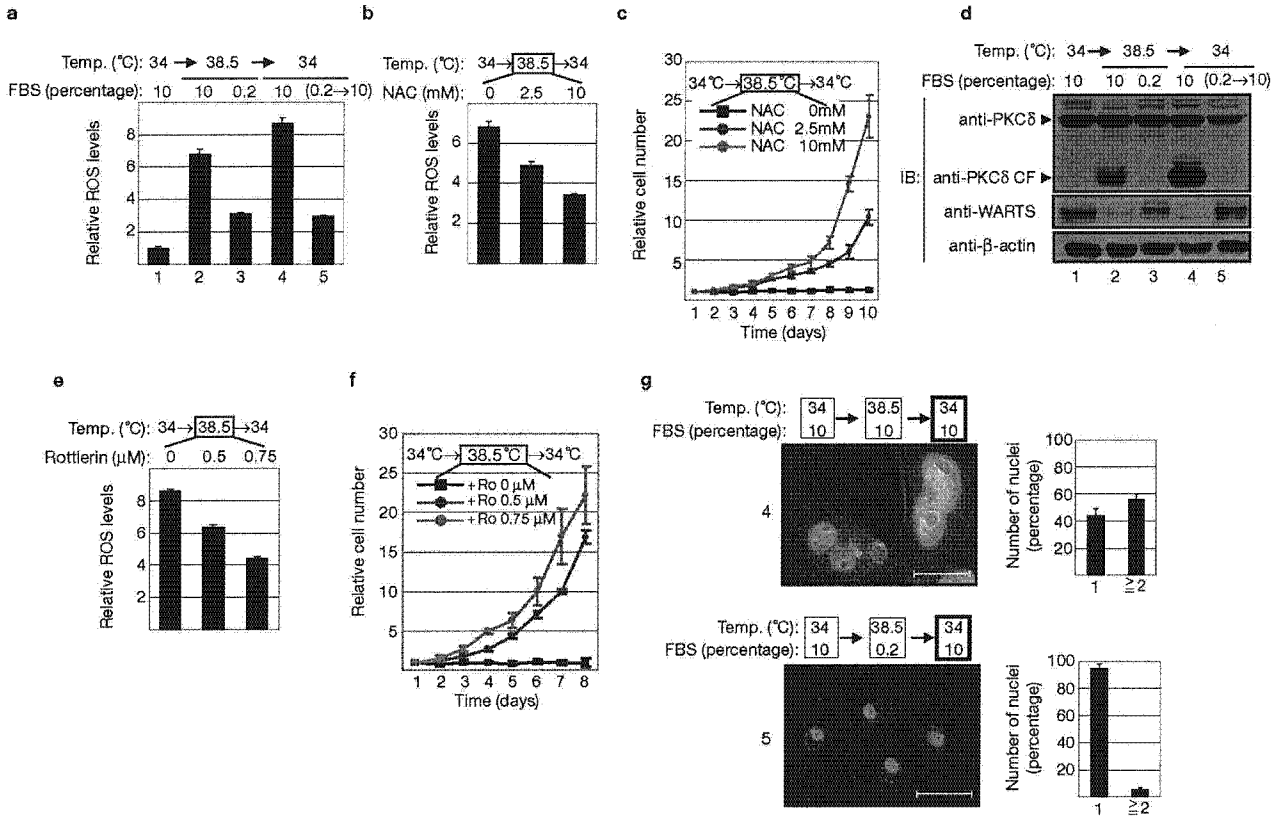


**Figure 2** Involvement of ROS–PKCδ signalling in irreversible cell-cycle arrest. (**a**) SVts8 cells were cultured as described in Fig. 1a (lane number corresponds to culture condition) and relative ROS levels at the indicated times were measured by DCF-DA staining. (**b**, **c**) SVts8 cells were cultured at 38.5 °C for 5 days in normal serum medium with NAC at the doses indicated. These cells were subsequently incubated at 34 °C for 5 days in normal serum medium without NAC. Cells were then subjected to analysis of relative ROS levels (**b**) or to cell proliferation assay performed in triplicate (**c**). The error bars indicate s.d. (**d**) SVts8 cells were cultured as described in Fig. 1a and protein expression at the indicated times was examined by western blotting using antibodies indicated. (**e**, **f**) SVts8 cells were cultured at 38.5 °C for 5 days in normal serum medium with rottlerin at the doses indicated. These cells were subsequently incubated at 34 °C in normal serum medium without rottlerin for 5 days. Cells were then subjected to analysis of relative ROS levels (**e**) or to cell proliferation assay performed in triplicate (**f**). The error bars indicate s.d. (**g**) Cells at the indicated times (4 and 5) in Fig. 1a were stained with DAPI. The histograms indicate the percentage of polynucleated cells. The error bars indicate s.d. The scale bars represent 50 μm.

subsequently inactivated, and correlated well with the levels of ROS (Fig. 2a, d and see Supplementary Information, Fig. S1f). Furthermore, treatment with rottlerin, a selective PKCδ inhibitor, throughout the incubation at 38.5 °C in normal serum medium enabled SVts8 cells to reinitiate cell proliferation on shifting the temperature to 34 °C in fresh normal serum medium. Notably, this was accompanied by a substantial reduction in the levels of ROS (Fig. 2e, f), indicating that PKCδ indeed has a key role in the maintenance of ROS production in senescent cells.

As it has previously been shown that PKCδ may have the potential to block cytokinesis[24], we next examined the morphology and cell-cycle profiles of irreversibly arrested SVts8 cells. A dramatic increase in polynucleated cells was observed when the temperature was shifted to 34 °C after 5 days culture at 38.5 °C in normal serum medium (Fig. 2g and see Supplementary Information, Fig. S2a), indicating that these cells are likely to have severe defects in cytokinesis. Such abnormal phenotypes were not observed if cells were cultured in low serum medium throughout the incubation at 38.5 °C (Fig. 2g and see Supplementary Information, Fig. S2a). Intriguingly, the levels of WARTS were inversely correlated with those of PKCδ-CF in SVts8 cells (Fig. 2d). Moreover, inhibition of ROS production by NAC treatment throughout the incubation at 38.5 °C resulted in marked recovery of the level of WARTS (Fig. 3a). Conversely, the levels of activated caspase-3, a known activator of PKCδ[6], and PKCδ-CF were diminished (Fig. 3a). Similar results were also observed when rottlerin was used instead of NAC (Fig. 3b). In contrast, treatment with $H_2O_2$ to increase the intracellular levels of ROS caused an activation of caspase-3, a significant induction of PKCδ activity, a remarkable reduction in WARTS expression and a senescent-like cell-cycle arrest in SVts8 cells (Fig. 3c and see Supplementary Information, Fig. S2b–e). Furthermore, ectopic expression of PKCδ–CF had similar effects in SVts8 cells at 34 °C (Fig. 3d, e). Taken together, these results strongly suggest that PKCδ is an upstream regulator of WARTS expression and has positive feedback effects on ROS production in senescent cells.

Unlike HDFs, PKCδ-CF was not induced during replicative senescence in MEFs (data not shown). However, treatment with $H_2O_2$ led to a substantial induction in PKCδ–CF and concomitant reduction of WARTS in wild-type MEFs, but not in MEFs lacking the *PKCδ* gene (see Supplementary Information, Fig. S2f)[25]. These results further support the role of PKCδ in enforcing stable cell-cycle arrest (see Supplementary Information, Fig. S2g–i). It is noteworthy that the reduction in WARTS was attenuated by the addition of MG132, a proteasome inhibitor

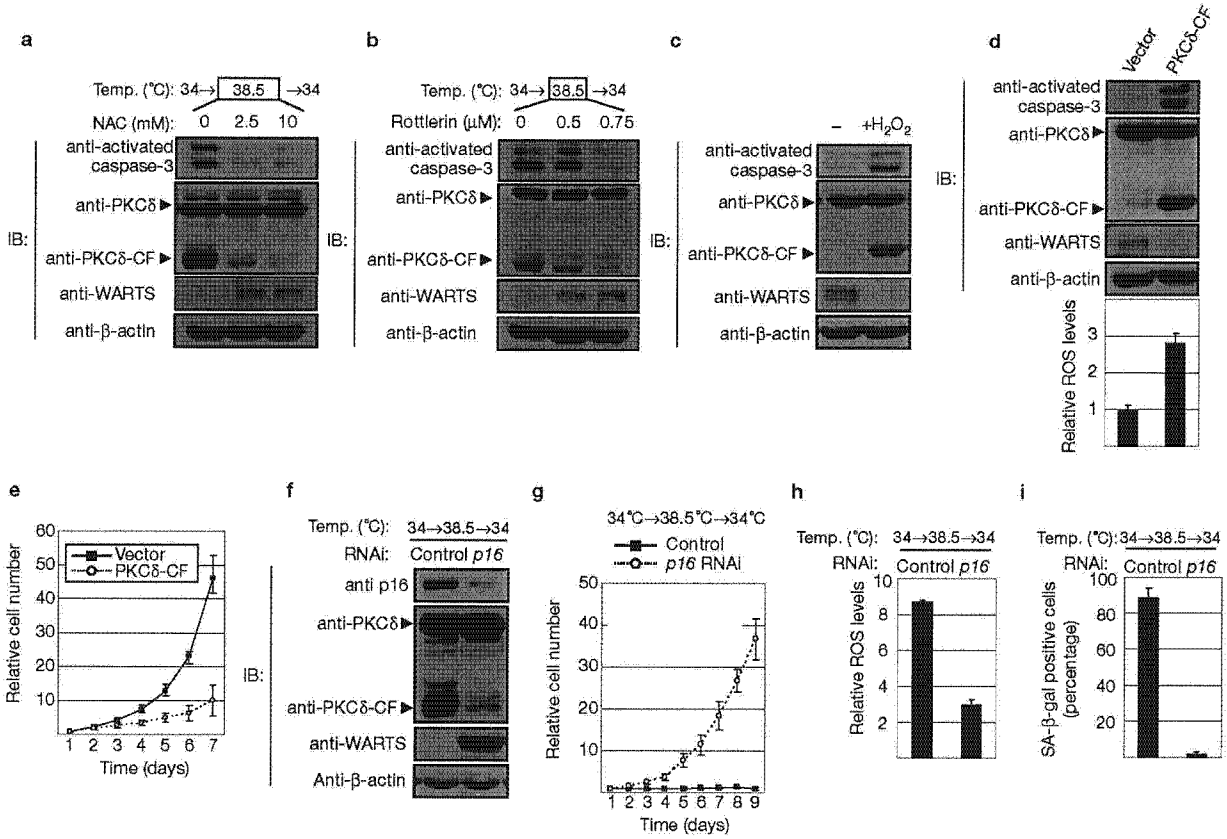


**Figure 3** Downregulation of WARTS by PKCδ. (**a**) SVts8 cells were cultured at 38.5 °C for 5 days in normal serum medium with NAC at the doses indicated. These cells were subsequently incubated at 34 °C for 5 days in normal serum medium without NAC. Cells were then subjected to western blotting with antibodies indicated. (**b**) SVts8 cells were cultured at 38.5 °C for 5 days in normal serum medium with Rottlerin at the doses indicated. These cells were subsequently incubated at 34 °C in normal serum medium without Rottlerin for 5 days. Cells were then subjected to western blotting with the antibodies indicated. (**c**) SVts8 cells cultured at 34 °C were treated with $H_2O_2$ as previously described[31]. Cells were then subjected to western blotting analysis using the antibodies indicated. (**d**, **e**) SVts8 cells were infected with retrovirus encoding PKCδ-CF or control vector at 34 °C. Cells were then subjected to analysis of relative ROS level, western blotting using the antibodies indicated (**d**) or to cell proliferation assay performed in triplicate at 34 °C in normal serum medium (**e**). The error bars represent s.d. (**f**, **i**) SVts8 cells were infected with retrovirus encoding RNAi against *p16*$^{INK4a}$ or control[26] at 34 °C. Cells were then incubated at 38.5 °C in normal serum medium for 5 days and subsequently incubated at 34 °C in fresh normal serum medium for another 5 days. Cells were then subjected to western blotting using the antibodies indicated (**f**), cell proliferation assay performed in triplicate (**g**), analysis of relative ROS levels (**h**) or to SA-β-gal assay (**i**). The error bars represent s.d.

(see Supplementary Information, Fig. S3a). However, mutation of the consensus sequence for phosphorylation by PKCδ (Ser 464 to Ala) did not alter the stability of WARTS in senescent cells (see Supplementary Information, Fig. S3b), suggesting that PKCδ may regulate the stability of WARTS indirectly through phosphorylating protein(s) controlling the stability of WARTS. It is also worth emphasizing that reduction of the levels of p16$^{INK4a}$ using RNA interference (RNAi)[26] diminished activation of ROS–PKCδ signalling and enabled SVts8 cells to reinitiate cell proliferation on shifting the temperature to 34 °C from 38.5 °C (Fig. 3f–i). Taken together, these data and previous reports showing that p16$^{INK4a}$ can initiate an autonomous senescence programme[14,15], indicate that the p16$^{INK4a}$–Rb pathway ensures the irreversibility of senescent cell-cycle arrest, at least in part through activating ROS–PKCδ signalling.

To ascertain the role of the ROS–PKCδ signalling pathway in primary human cells, we examined whether the ROS–PKCδ signalling pathway was activated in Ras-induced senescent HDFs[27,28]. The levels of ROS and PKCδ-CF were significantly increased and the level of WARTS was significantly reduced in Ras-induced senescent TIG-3 cells and in Hs68 cells (Fig. 4a, b and see Supplementary Information, Fig. S3c). Importantly, subsequent expression of large T antigen was unable to revoke ROS–PKCδ signalling or cell-cycle arrest in Ras-induced senescent TIG-3 cells, despite its ability to induce DNA synthesis (see Supplementary Information, Fig. S3d–g), indicating that ROS–PKCδ signalling pathway does serve as an additional level of security to prevent cell-cycle re-entry in senescent primary human cells. As shown by the experiments in Fig. 3d, overexpression of PKCδ–CF alone strikingly reduced the level of WARTS and blocked cell proliferation in early passage TIG-3 cells (Fig. 4a, c). Significantly, the arrested cells displayed phenotypic features of cellular senescence (Fig.4d). Moreover, overexpression of PKCδ-CF itself substantially elevated the levels of ROS and activated caspase-3 in early passage TIG-3 cells (Fig. 4b and see Supplementary Information, Fig. S3h), demonstrating that PKCδ also has positive feedback effects on ROS production in primary human cells. Interestingly, the levels of ROS induced by overexpression of PKCδ-CF were remarkably attenuated when cells were treated with DPI (see Supplementary Information, Fig. S3i), suggesting that NADPH oxidase is implicated in this setting.

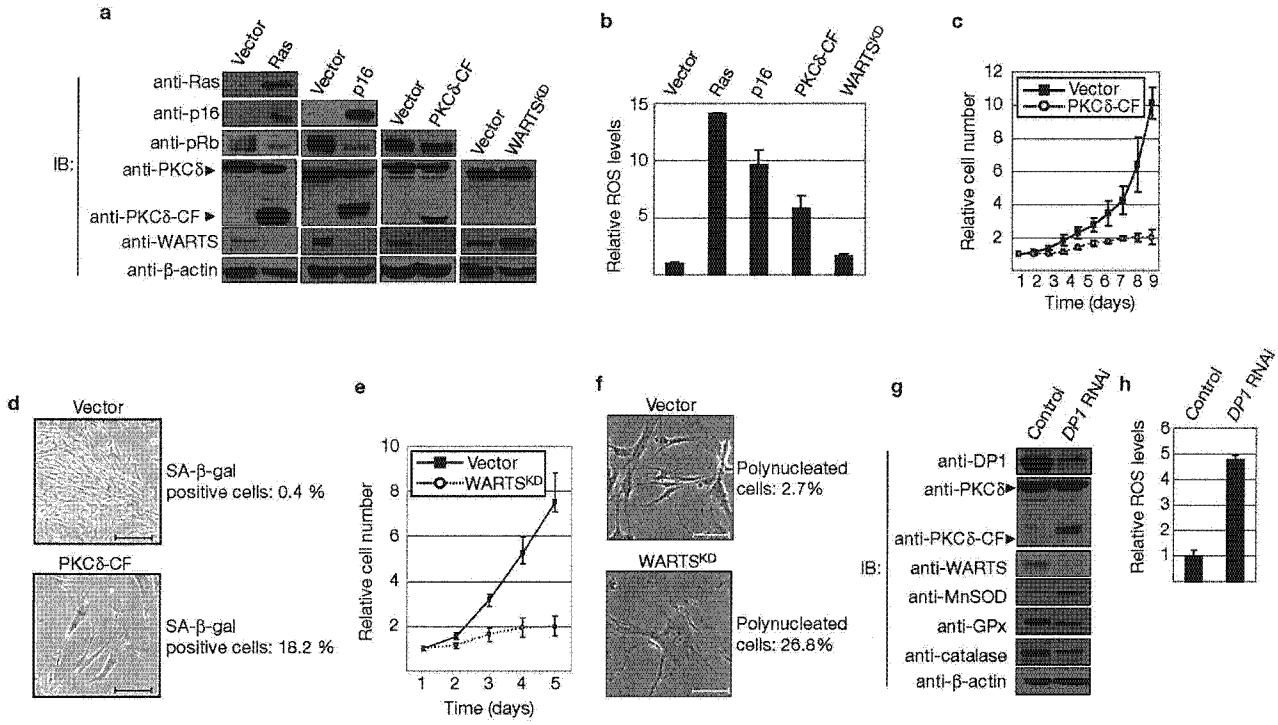


**Figure 4** p16$^{INK4a}$–Rb pathway elicits ROS–PKCδ signalling in primary human diploid fibroblasts. (**a–f**) Early passage (40 population doublings level; PDL) TIG-3 cells were infected with retrovirus encoding oncogenic Ras (Ras), p16$^{INK4a}$, PKCδ-CF, WARTS$^{KD}$ (ref. 9) or control empty vector. Cells were then subjected to western blotting with antibodies indicated (**a**), or to analysis of intracellular levels of ROS (**b**). TIG-3 cells infected with retrovirus encoding PKCδ-CF or control empty vector were subjected to cell proliferation assay in triplicate (**c**) and to SA-β-gal analysis (**d**). TIG-3 cells infected with retrovirus encoding WARTS$^{KD}$ or control empty vector were subjected for cell proliferation assay performed in triplicate (**e**). Representative images of the indicated cells are shown (**f**). (**g, h**) Early passage (40 PDL) TIG-3 cells were infected with retrovirus encoding RNAi against *DP1*[29] or control sequence. After selection with antibiotics, cells were then subjected to western blotting with the antibodies indicated (**g**) or to analysis of intracellular levels of ROS (**h**). These assays were performed in triplicate and representative results are shown in **g**. The error bars represent s.d. The scale bars represent 200 μm in **d** and 100 μm in **f**.

Overexpression of a dominant negative form of WARTS (WARTS$^{KD}$)[9] did not increase the level of ROS or PKCδ-CF (Fig. 4a, b), but significantly inhibited cell proliferation accompanied by a substantial increase in polynucleated TIG-3 cells (Fig 4e, f), as previously reported[9–11]. These results therefore indicate that a reduction in WARTS expression is, at least partly responsible for the cytokinetic block in senescent cells.

To obtain a mechanistic insight into how p16$^{INK4a}$–Rb-pathway promotes ROS production, we next examined the effects of the reduction of the level of DP1, an essential activator of the E2F transcription factor, by RNA interference (RNAi)[29]. Interestingly, reduction of the level of DP1 led to a significant increase in the levels of ROS and PKCδ-CF expression and substantial reduction in WARTS expression in TIG-3 cells (Fig. 4g, h). Notably, the level of manganese superoxide dismutase (MnSOD) expression was increased, whereas those of glutathione peroxidases (GPX) and catalase expression were slightly decreased in *DP1*-knockdown cells (Fig. 4g). Thus, it is possible that more and more superoxide radicals are converted to $H_2O_2$ but are not detoxified to water and oxygen, resulting in accumulation of $H_2O_2$, a part of ROS, in *DP1*-knockdown cells. These results are consistent with a previous report showing that overexpression of MnSOD increases the levels of ROS[30]. Taken together, our results strongly suggest that the p16$^{INK4a}$–Rb pathway provokes ROS–PKCδ signalling through blocking the E2F activity.

To further extend these findings to replicative senescence, ROS–PKCδ signalling was examined in late passage TIG-3 cells. TIG-3 cells lose their proliferative activity and senesce at around 79 population doublings. These cells were classed as 'early senescent' and were cultured for a further 3 weeks before being classed as 'late senescent'. Although lentivirus mediated large T antigen expression enabled early-senescent cells to reinitiate DNA synthesis and cell proliferation, a similar level of large T antigen expression was unable to stimulate cell proliferation in late-senescent cells (Fig. 5a, b). Importantly, the levels of p16$^{INK4a}$, ROS and PKCδ-CF in late-senescent cells were significantly higher than those in early-senescent cells (Fig. 5c, d). Consistent with these results, the level of WARTS was strikingly reduced in late-senescent cells (Fig. 5c) and these levels were unchanged even when large T antigen was subsequently expressed in late-senescent cells (Fig. 5c, d), indicating that ROS–PKCδ signalling pathway does have a role in replicative senescence. It is also interesting to note that the levels of proteins involved in cytokinesis that we tested were all reduced in late-senescent cells (Fig. 5c). However, the expression levels of these proteins, with the exception of WARTS, returned to the original levels when large T antigen was expressed (Fig. 5c), illustrating the importance of WARTS as a critical downstream target of ROS–PKCδ signal in late senescence.

As we were unable to recover the level of WARTS by ectopic expression in senescent cells (see Supplementary Information, Fig. S3b), it is still unclear whether WARTS is the most critical downstream target of the ROS–PKCδ signalling pathway towards the cytokinetic block in senescent cells. It is possible that PKCδ may have other targets to

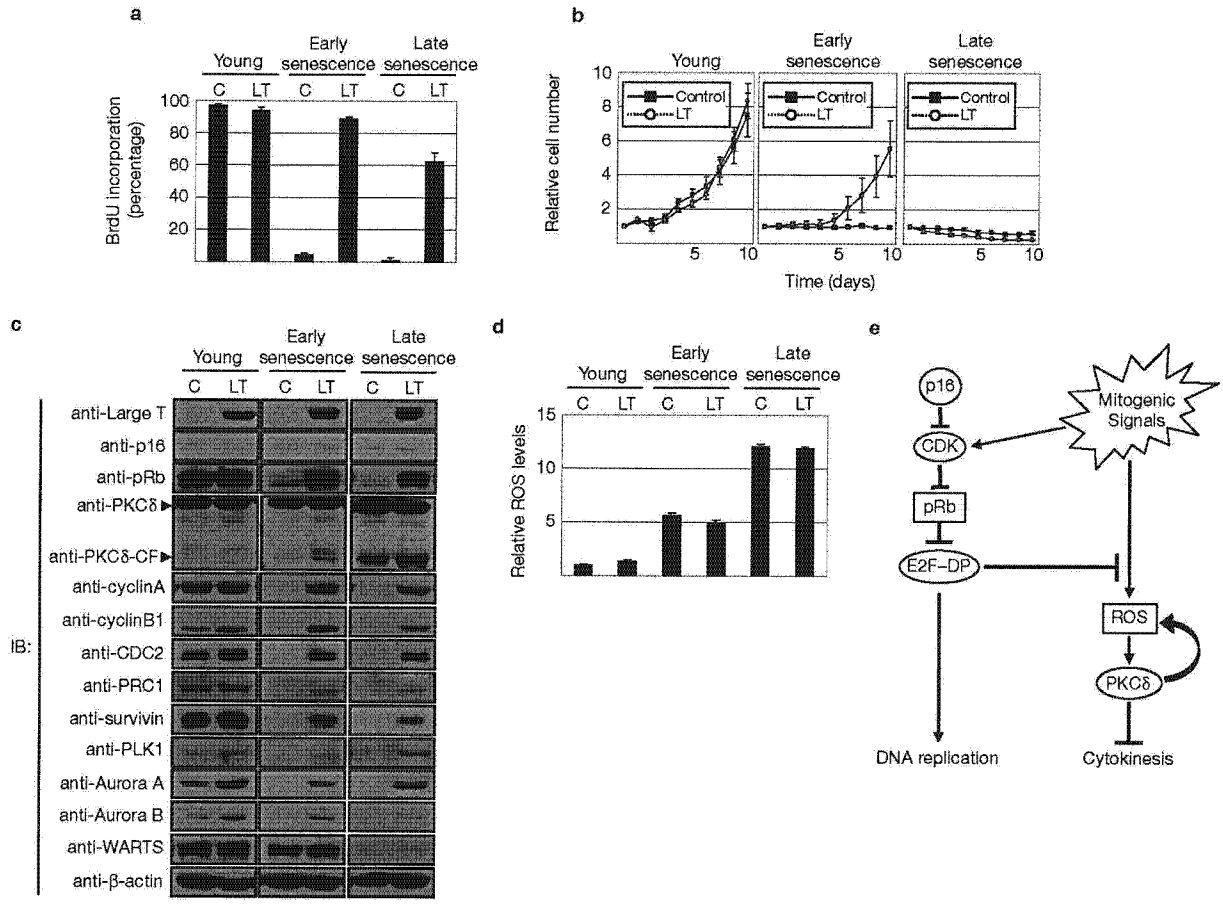


**Figure 5** Irreversibility of replicative senescence. (**a–d**) Young (early passage), early-senescent or late-senescent TIG-3 cells were infected with lentivirus encoding either SV40 large T antigen (LT) or GFP (control). Five days later, these cells were subjected to BrdU incorporation analysis (**a**), cell proliferation analysis (**b**), western blotting using the indicated antibodies (**c**) or to assay for intracellular levels of ROS (**d**) as described in Fig. 2. These assays were performed in triplicate and representative results are shown in **c**. The error bars represent s.d. (**e**) Dual roles for the $p16^{INK4a}$–Rb pathway in senescent cell-cycle arrest. In proliferating cells, the effects of mitogenic signals in ROS production are counterbalanced by E2F–DP activity. However, when E2F–DP activity is shut down by fully activated pRb, mitogenic signalling, in turn, increases the level of ROS and elicits a positive feedback activation of ROS–PKCδ signalling pathway. Elevated levels of $p16^{INK4a}$ therefore establish an autonomous activation of ROS–PKCδ signalling, leading to an irrevocable block to cytokinesis in human senescent cells.

enforce the cytokinetic block[22]. However, overexpression of a dominant negative form of WARTS, on its own, significantly inhibited cell proliferation accompanied by a substantial increase in polynucleated cells (Fig. 4e, f). These results, together with previous reports showing that WARTS is a MEN-kinase required for cytokinesis[9–11], strongly suggest that reduction of WARTS is, at least partly responsible for cytokinetic block in senescent cells. Together, our data reveal a novel function for the $p16^{INK4a}$–Rb pathway operating in human cell senescence (Fig. 5e). This system may serve as a fail-safe mechanism, especially in case of the accidental inactivation of pRb and p53 in human senescent cells. □

## METHODS

**Cells and cell culture.** Normal human diploid fibroblasts TIG-3 cells and HS68 cells were cultured in DME supplemented with 10% fetal bovine serum (FBS) at 37 °C[28]. SVts8 cells were cultured in DME supplemented with 10% FBS at 34 °C[17]. Early passage TIG-3 cells (40 population doublings) and Hs68 cells (45 population doublings) were used as young cells. Cell proliferation analysis and SA-βgal assay were performed as previously described[29].

**Viral infections.** TIG-3 cells and SVts8 cells were rendered sensitive to infection by ecotropic retroviruses as previously described[29] and infected with recombinant retroviruses encoding Ras V12 (in pBabe-puro)[27], PKCδ-CF (in pMarX-hygro)[6], p16 (in pMarX-hygro)[28], $WARTS^{KDK734A}$ (in pMarX-puro)[9], *p16* shRNA (in pRetrosuper-hygro)[26] or *DP1* shRNA (in pRetrosuper-puro)[29]. Pools of drug-resistant cells were analysed 7 days after infection. For lentiviral infection, senescent TIG-3 cells were infected with lentivirus encoding either large T antigen or GFP as previously described[14]. The infection efficiency (>99%) was monitored by GFP.

**Protein analysis.** Immunoblotting and immunoprecipitation were performed as previously described[28] with primary antibodies against aurora A (610938; BD Biosciences, San Jose, CA), aurora B (611082; BD), β-actin (sc-8432; Santa Cruz Biotechnology, Santa Cruz, CA), caspase-3 (9662; Cell Signalling, Beverley, MA), catalase (ab1877; Abcam, Cambridge, UK), cdc2 (#17; Cancer Research UK, London, UK), cyclin A (sc-751; Santa Cruz), cyclin B1 (sc-752; Santa Cruz), DP1 (11834; Abcam), GPX (mo15-3; MBL, Nagoya, Japan), large T antigen (L-19)[17], MnSOD (611580; BD), PKCδ (sc-937; Santa Cruz), PLK1 (06-813; Upstate, Lake Placid, NY), PRC1 (gift from W. Jiang, Burnham Insititute, La Jolla, CA), p16 (Ab-1; Oncogene, Boston, MA), p21 (sc-397; Santa Cruz), p53 (Ab-6; Calbiochem, San Diego, CA), Ras (Ab-4; Oncogene), RB (sc-102; Santa Cruz and 554136;

BD), survivin (AF886; R&D Systems, Minneapolis, MN) and WARTS (C-2)[9]. In some experiments, cells were incubated with 10 μM MG132 (Calbiochem) for 12 h before harvest.

**Analysis of intracellular ROS.** To assess the generation of intracellular ROS levels, cells were incubated with 20 μM DCF-DA (Calbiochem) for 20 min at 37 °C. The peak excitation wavelength for oxidized DCF was 488 nm and for emission was 525 nm.

**Protein kinase assay.** Immune complex kinase assay was performed as previously described[23] with antibody against PKCδ (sc-937; Santa Cruz). The incubation was carried out for 5 min or 30 min at 30 °C.

*Note: Supplementary Information is available on the Nature Cell Biology website.*

ACKNOWLEDGEMENTS

We thank D. Mann, G. Peters, J. Campisi and U. Kikkawa for helpful comments on the manuscript; R. Agami for providing *p16* knockdown construct; D. Beach and G. Hannon for providing pMarX retrovirus vector; W. Jiang and R. Fukunaga for providing anti-PRC1 antibody; and D. Kufe and S. Ohno for *PKCδ* cDNA. We also thank A. Hirao for his useful suggestion in analysis of intracellular ROS. This work was supported by grants from Ministry of Education, Science, Sports and Technology of Japan, Ministry of Health, Labour and Welfare of Japan, the Uehara Memorial Foundation, the Sumitomo Foundation, the Nakatomi Foundation, the Sagawa Foundation for Promotion of Cancer Research, the Inamori Foundation and Sankyo Foundation of Life Science (E.H.). A.T. is supported by the Japan Society for the Promotion of Science.

COMPETING FINANCIAL INTERESTS

The authors declare that they have no competing financial interests.

Published online at http://www.nature.com/naturecellbiology/
Reprints and permissions information is available online at http://npg.nature.com/reprintsandpermissions/

1. Lowe, S. W., Cepero, E. & Evan, G. Intrinsic tumour suppression. *Nature* **432**, 307–315 (2004).
2. Sharpless, N. E. & DePinho, R. A. Cancer: crime and punishment. *Nature* **436**, 636–637 (2005).
3. Serrano, M. & Blasco, M. A. Putting the stress on senescence. *Curr. Opin. Cell Biol.* **13**, 748–753 (2001).
4. Drayton, S. & Peters, G. Immortalisation and transformation revisited. *Curr. Opin. Genet. Dev.* **12**, 98–104 (2002).
5. Herbig, U. & Sedivy, J. M. Regulation of growth arrest in senescence: telomere damage is not the end of the story. *Mech. Ageing & Dev.* **127**, 16–24 (2006).
6. Ghayur, T. *et al.* Proteolytic activation of protein kinase C δ by an ICE/CED 3-like protease induces characteristics of apoptosis. *J. Exp. Med.* **184**, 2399–2404 (1996).
7. Bey, E. A. *et al.* Protein kinase Cδ is required for $p47^{phox}$ phosphorylation and translocation in activated human monocytes. *J. Immunol.* **173**, 5730–5738 (2004).
8. Talior, I., Tennenbaum, T., Kuroki, T. & Eldar-Finkelman, H. PKC-δ-dependent activation of oxidative stress in adipocytes of obese and insulin-resistant mice: role for NADPH oxidase. *Am. J. Physiol. Endocrinol. Metab.* **288**, E405–E411 (2005).
9. Iida, S. *et al.* Tumor suppressor WARTS ensures genomic integrity by regulating both mitotic progression and G1 tetraploidy checkpoint function. *Oncogene* **23**, 5266–5274 (2004).
10. Yang, X. *et al.* LATS1 tumour suppressor affects cytokinesis by inhibiting LIMK1. *Nature Cell Biol.* **6**, 609–617 (2004).
11. Bothos, J., Tuttle, R. L., Ottey, M., Luca, F. C. & Halazonetis, T. D. Human LATS1 is a mitotic exit network kinase. *Cancer Res.* **65**, 6568–6575 (2005).
12. Sage, J., Miller, A. L., Perez-Mancera, P. A., Wysocki, J. M. & Jacks, T. Acute mutation of retinoblastoma gene function is sufficient for cell cycle re-entry. *Nature* **424**, 223–228 (2003).
13. Dirac, A. M. & Bernards, R. Reversal of senescence in mouse fibroblasts through lentiviral suppression of p53. *J. Biol. Chem.* **278**, 11731–11734 (2003).
14. Beausejour, C. M. *et al.* Reversal of human cellular senescence: roles of the p53 and p16 pathways. *EMBO J.* **22**, 4212–4222 (2003).
15. Dai, C. Y. & Enders, G. H. $p16^{INK4a}$ can initiate an autonomous senescence program. *Oncogene* **19**, 1613–1622 (2000).
16. Gorman, S. D. & Cristofalo, V. J. Reinitiation of cellular DNA synthesis in BrdU-selected nondividing senescent WI-38 cells by simian virus 40 infection. *J. Cell. Physiol.* **125**, 122–126 (1985).
17. Tahara, H., Sato, E., Noda, A. & Ide, T. Increase in expression level of p21sdi1/cip1/waf1 with increasing division age in both normal and SV40-transformed human fibroblasts. *Oncogene* **10**, 835–840 (1995).
18. Lloyd, A. C. Limits to lifespan. *Nature Cell Biol.* **4**, E25–E27 (2002).
19. Satyanarayana, A. *et al.* Mitogen stimulation cooperates with telomere shortening to activate DNA damage responses and senescence signaling. *Mol. Cell. Biol.* **24**, 5459–5474 (2004).
20. Irani, K. *et al.* Mitogenic signaling mediated by oxidants in Ras-transformed fibroblasts. *Science*, **275**, 1649–1652 (1997).
21. Lee, A. C. *et al.* Ras proteins induce senescence by altering the intracellular levels of reactive oxygen species. *J. Biol. Chem.* **274**, 7936–7940 (1999).
22. Wheaton, K. & Riabowol, K. Protein kinase C δ blocks immediate-early gene expression in senescent cells by inactivating serum response factor. *Mol. Cell. Biol.* **24**, 7298–7311 (2004).
23. Konishi, H. *et al.* Activation of protein kinase C by tyrosine phosphorylation in response to $H_2O_2$. *Proc. Natl Acad. Sci. USA* **94**, 11233–11237 (1997).
24. Watanabe, T. *et al.* Cell division arrest induced by phorbol ester in CHO cells overexpressing protein kinase C-δ subspecies. *Proc. Natl Acad. Sci. USA* **89**, 10159–10163 (1992).
25. Miyamoto, A. *et al.* Increased proliferation of B cells and auto-immunity in mice lacking protein kinase Cδ. *Nature* **416**, 865–869 (2002).
26. Voorhoeve, P. M. & Agami, R. The tumor-suppressive functions of the human INK4A locus. *Cancer Cell* **4**, 311–319 (2003).
27. Serrano, M., Lin, A. W., McCurrach, M. E., Beach, D. & Lowe, S. W. Oncogenic ras provokes premature cell senescence associated with accumulation of p53 and $p16^{INK4a}$. *Cell* **88**, 593–602 (1997).
28. Ohtani, N. *et al.* Opposing effects of Ets and Id proteins on $p16^{INK4a}$ expression during cellular senescence. *Nature* **409**, 1067–1070 (2001).
29. Maehara, K. *et al.* Reduction of total E2F/DP activity induces senescence-like cell cycle arrest in cancer cells lacking functional pRB and p53. *J. Cell Biol.* **168**, 553–560 (2005).
30. Behrend, L., Mohr, A., Dick, T. & Zwacka, R. M. Manganase superoxide dismutase induces p53-dependent senescence in colorectal cancer cells. *Mol. Cell. Biol.* **25**, 7758–7769 (2005).
31. Chen, J. H. *et al.* Loss of proliferative capacity and induction of senescence in oxidative stressed human fibroblasts. *J. Biol. Chem.* **279**, 49439–49446 (2004).

nature
cell biology



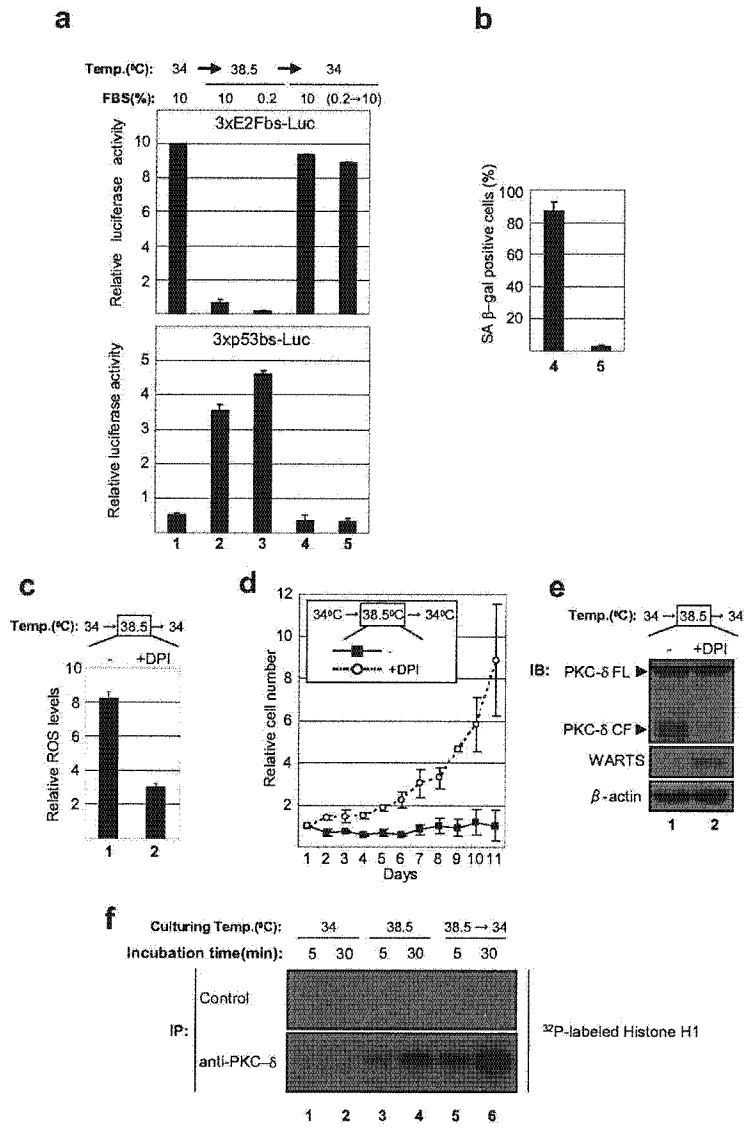


**Figure S1** Analysis of transcriptional control activity of pRb and p53 in Svts8 cells. **(a)** SVts8 cells were transfected with a reporter construct containing tandem repeat of E2F-responsive element (3XE2Fbs-Luc) or p53-responsive element (3Xp53bs-Luc) driving luciferase gene. After selection with antibiotics, pooled cells were then cultured as described in Fig. 1a (lane number corresponds to culture condition). Luciferase activities were assayed at indicated time points. Error bars indicate standard deviation (SD). **(b)** SVts8 cells were cultured as described in Fig. 1a (lane number corresponds to culture condition), and were subjected to analysis of SA-β gal activity at indicated time points. **(c-e)** SVts8 cells were cultured at 38.5$^0$C for 5 days in normal serum medium with (+DPI) or without (-) 0.2μM of DPI. These cells were subsequently incubated at 34$^0$C for 5 days in fresh normal serum medium without DPI. Cells were then subjected to analysis of ROS levels (c), cell proliferation assay performed in triplicate (d) or to Western blotting with antibodies indicated at left (e). **(f)** SVts8 cells were cultured in normal serum medium at 34$^0$C (lanes 1 and 2). Cells were then incubated at 38.5$^0$C for 5 days in normal serum medium (lanes 3 and 4), and were subsequently incubated at 34$^0$C in normal serum medium for another 5 days (lanes 5 and 6). Cell lysates were prepared at indicated time point and were precipitated with or without antibody against PKC-δ. Resulting complexes were incubated with Histone H1 as the substrate for 5 min (lanes 1, 3 and 5) or 30 min (lanes 2, 4 and 6) at 30$^0$C in the presence of [γ-$^{32}$P]ATP. Labeled proteins were resolved on denaturing polyacrylamide gels, which were dried and subjected to autoradiography.

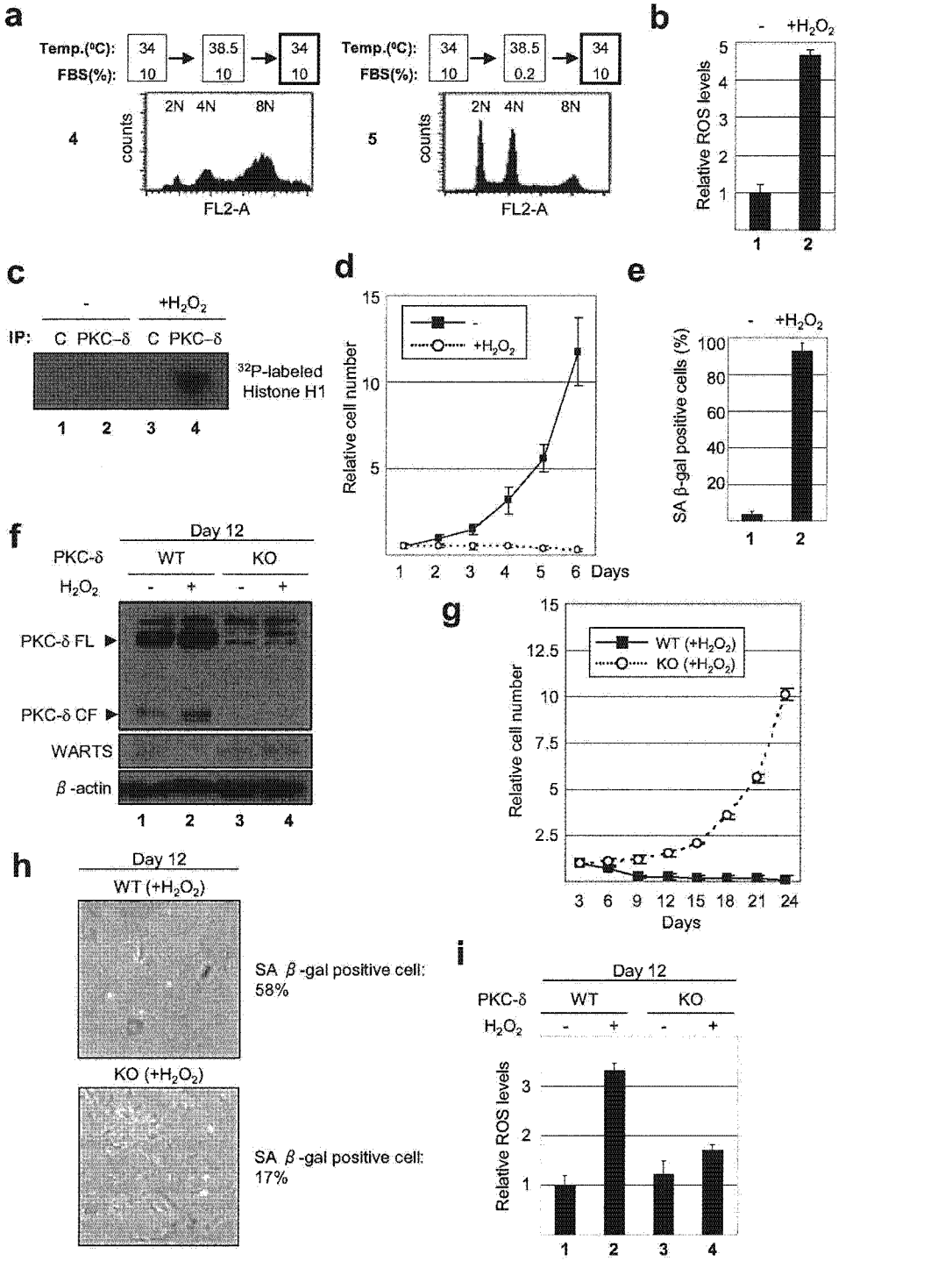


**Figure S2** Role of PKC-δ on H2O2-induced senescence-cell cycle arrest. **(a)** SVts8 cells were cultured as described in Fig. 1a. The DNA content of cells was measured by FACS analysis at indicated time points (4 and 5). **(b-e)** SVts8 cells cultured at 34 $^{0}$C were treated with H2O2 as described previously[31]. Cells were then subjected to analysis of ROS levels (b), PKC-δ kinase assay as described in Fig. S1f (c), cell proliferation assay performed in triplicate (d) or to SA-β-gal analysis (e). Error bars indicate SD. **(f-i)** Early passage MEFs lacking the PKC-δ gene (KO)[25] or control (WT) were cultured in DME containing 10% FBS at 37 $^{0}$C and were treated with (+) or without (-) H2O2 as described in panel b to e. Cells were then subjected to immunoblotting with antibodies shown left (f) or to cell proliferation assay in triplicate (g). Representative photographs of the cells stained for SA-β-gal activity at indicated time point (Day 12) were shown (h). Relative ROS levels were measured at day 12. Error bars indicate SD (i).

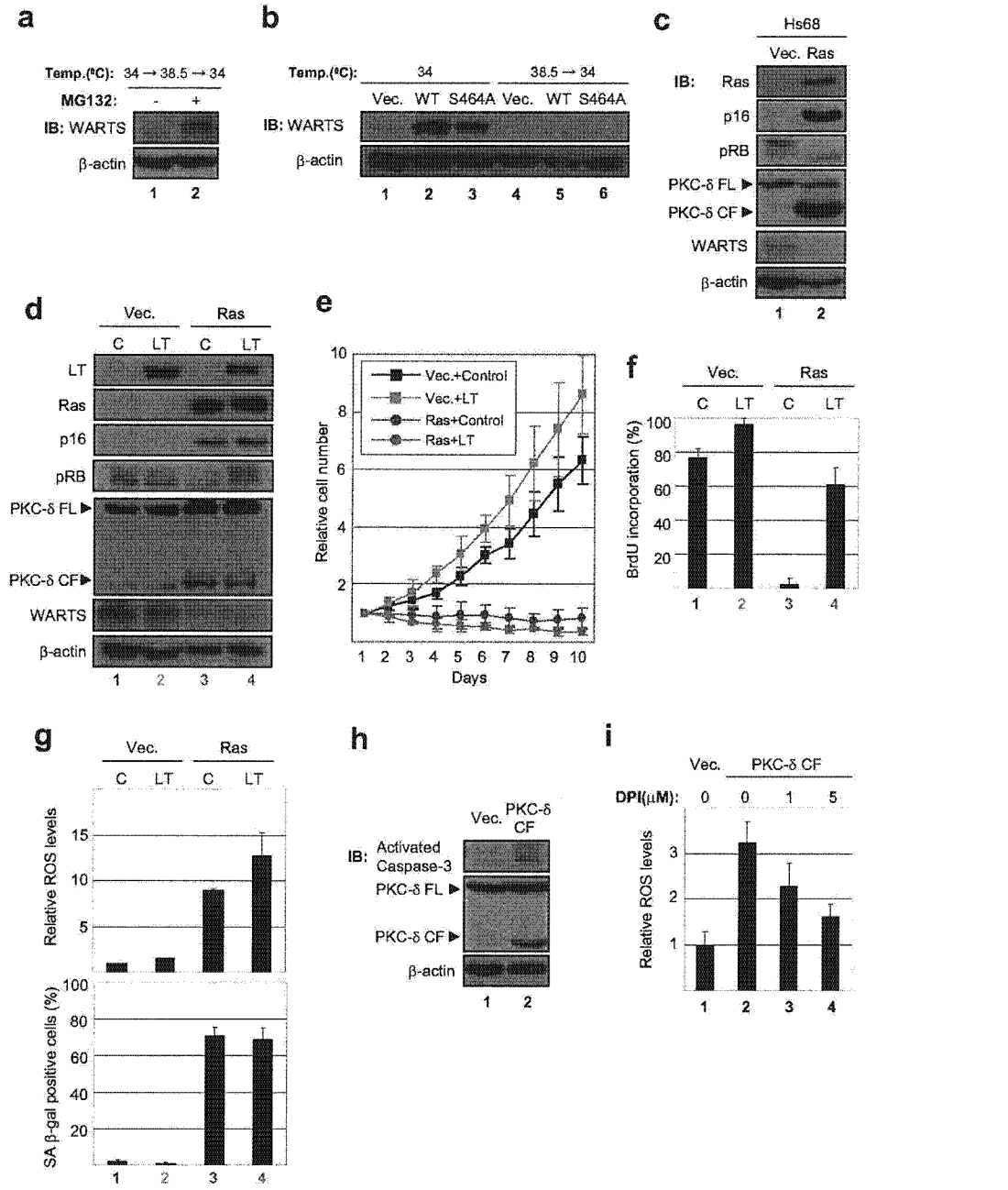


**Figure S3** ROS regulate irreversible cell cycle arrest. **(a)** SVts8 cells were cultured at 38.5$^0$C for 5days in normal serum medium. Cells were then incubated at 34$^0$C in normal serum medium for 5days and were subsequently incubated with (lane 2) or without (lane 1) 10 μM of MG132 for 12 hrs. Cells were then subjected to western blotting using antibodies shown left. **(b)** SVts8 cells were infected with retrovirus encoding wild type WARTS (WT), S464A mutant (S464A) or vector control (Vec). Infected cells were cultured at 34$^0$C in normal serum medium (lanes 1 to 3). These cells were then cultured at 38.5C for 5 days in normal serum medium, and were subsequently incubated at 34$^0$C in normal serum medium for another 5 days (lanes 4 to 6). Expression levels of WARTS were measured by Western blotting using antibodies indicated at left. **(c)** Ras provokes ROS/PKC-δ signalling pathway in Hs68 cells. Early passage (45PDL) primary human skin fibroblast, Hs68 cells, were infected with retrovirus encoding oncogenic Ras or control empty vector. Cells were then subjected to immunoblotting with antibodies indicated at left. **(d-g)** Early passage (40PDL) TIG-3 cells were infected with retrovirus encoding oncogenic Ras or control empty vector (Vec). When senescence-like cell cycle arrest was induced, cells were subsequently infected with lentivirus encoding SV40 large T antigen (LT) or GFP as a control. Cells were then subjected to immunoblotting with antibodies indicated at left (d), cell proliferation assay (e), BrdU incorporation assay (f) or to ROS and SA-β-gal analysis (g). These assays were performed in triplicate and representative results were shown in panel d. Error bars indicate SD. **(h)** Early passage (40PDL) TIG-3 cells were infected with retrovirus encoding PKC-δ CF or control empty vector (Vec.), as described in Fig. 4. Cells were then subjected to Western blotting with antibodies indicated at left. **(i)** TIG-3 cells expressing exogenous PKC-δ CF were treated with DPI for 24hrs at the doses indicated. These cells were then subjected to analysis of relative ROS levels. Error bars indicate SD.

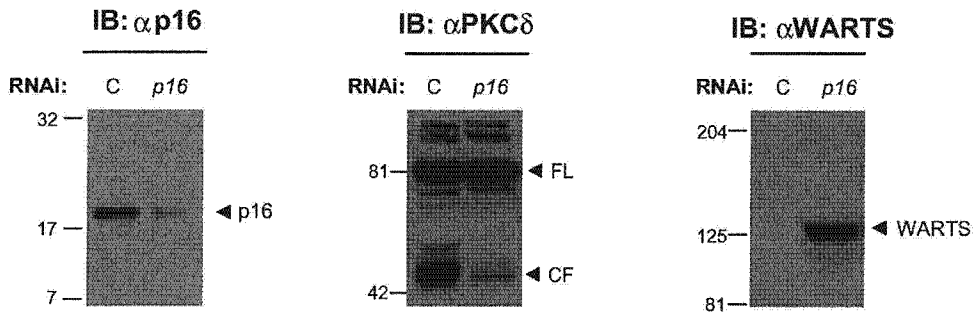


**Expanded blots including molecular weight size markers from Fig.3f**

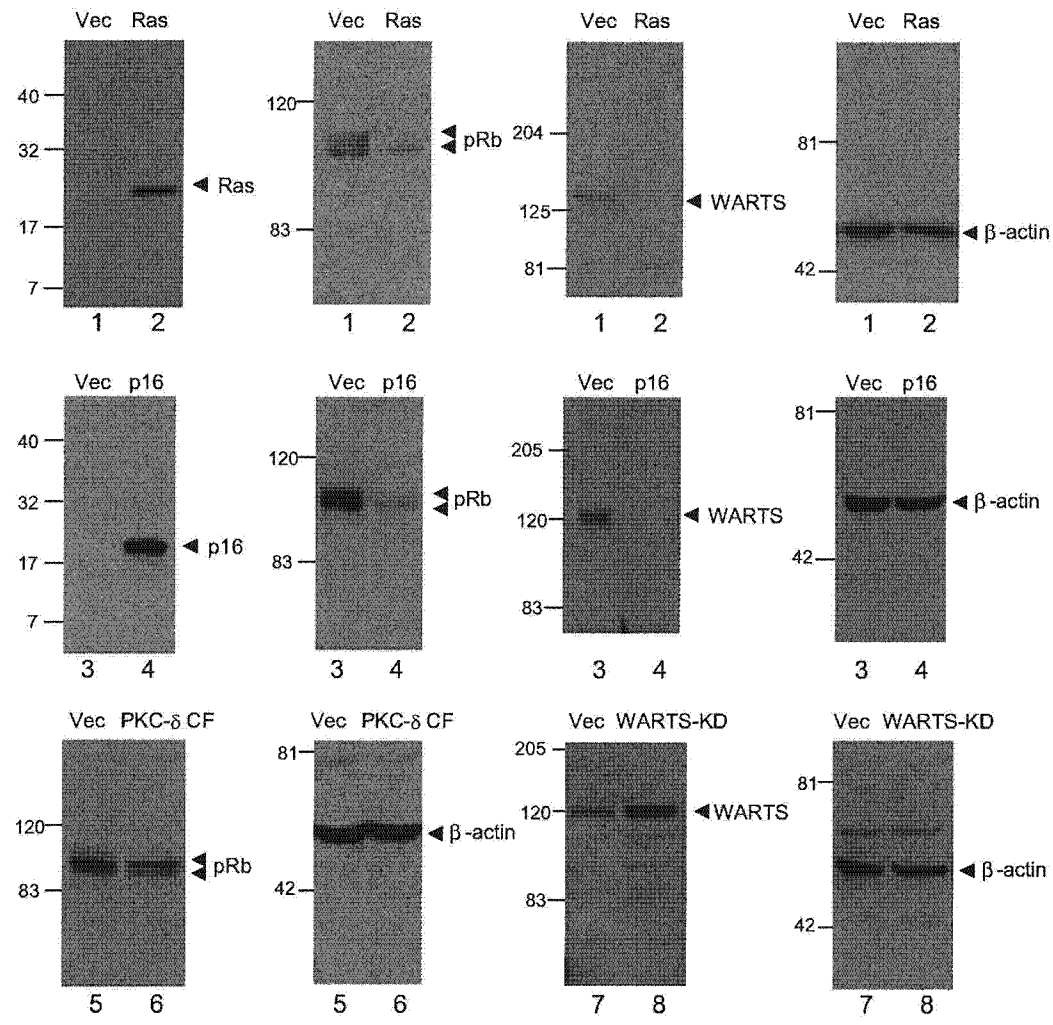


**Expanded blots including molecular weight size markers from Fig.4a**